Microscale investigations of the fate of heavy metals associated to iron-bearing particles in a highly polluted stream

Emmanuelle Montarges-Pelletier, Caroline Duriez, Jaafar Ghanbaja, Laurent Jeanneau, Gerard Falkenberg, Laurent J. Michot

Micro-scale investigations of the fate of heavy metals associated to iron-bearing particles in a highly polluted stream.

MONTARGES-PELLETIER Emmanuelle[1,2], DURIEZ Caroline[1,2], GHANBAJA Jaafar[3,4], JEANNEAU Laurent[5], FALKENBERG Gerard[6], MICHOT Laurent J.[1,2,7]

1-Laboratoire Interdisciplinaire des Environnements Continentaux, CNRS UMR 7360, 15 avenue du Charmois, BP 40, 54500 Vandoeuvre-les-Nancy, France

33 3 83 59 62 52 - 33 3 83 59 62 55 emmanuelle.montarges@univ-lorraine.fr.

2-Laboratoire Interdisciplinaire des Environnements Continentaux, Université de Lorraine, 15 avenue du Charmois, BP 40, 54500 Vandoeuvre-les-Nancy, France

3-CC-MEM, Institut Jean Lamour, Université de Lorraine, Parc de Saurupt CS 50840, 54011 Nancy cedex, France

4-CC-MEM, Institut Jean Lamour, CNRS UMR 7198, Parc de Saurupt CS 50840, 54011 Nancy cedex, France

5-Geosciences Rennes, CNRS Université de Rennes 1, Bâtiment 28, Beaulieu, 263 avenue du général Leclerc, 35042 RENNES cedex, France.

6-Hamburger Synchrotronstrahlungslabor (HASYLAB) at DESY, Notkestr. 85, D-22603 Hamburg, Germany

7-present address Physicochimie des Electrolytes, Colloïdes et Sciences Analytiques UMR 7195 - CNRS - UPMC – ESPCI, 4 place Jussieu, 75005 PARIS, France.

Abstract

As it flows through a dense steel making area, the Fensch River does transport iron-rich particles and colloids, displaying high contents in metallic contaminants (Zn, Cr, Pb, Cu, Ni, As). Chemical analysis using ICP-MS was carried out on three compartments, waters, suspended material and sediments, along the river linear. The variations of metallic trace elements concentrations along the river, were shown to being partially related to external inputs (industrial and domestic waste waters, urban surfaces leaching). However, some discrepancies of elements partitioning were evidenced. Pb, Cu, Mn tend to concentrate in suspended particulate and in dissolved fraction, while Cr and As follow Fe trend and concentrate within sediments of the most downstream station, just before the junction with Moselle waters. Zn appears strongly associated to iron rich-particles, resulting in a decrease of its concentration in waters for the last station. Along the Fensch linear, the variation of metal partitioning between water and particulate phases is accompanied with strong modifications of nature and mineralogy of iron-rich particles, as evidenced by microanalyses using electron and X-ray beams. The combination of bulk analyses using ICP-MS

and microanalyses, applied to the three compartments allowed us to propose a three step process "settling-weathering-resuspension" to explain the Zn partitioning.

river particles, metallic contaminants, iron, micro-spectroscopy, microanalyses

Introduction

Metallic pollution in aquatic systems represents a major environmental concern due to the persistence and toxicity of heavy metals. Studies on metal-degraded aquatic systems should include the analysis of metal contents and speciation in at least three compartments, the dissolved fraction, the sediments and the suspended solids (particles and colloids) that have been shown to play a major role in the transport and speciation of toxic substances (Mavrocordatos et al. 2007; McCarthy and Zachara 1989; Stumm 1993; Warren and Zimmermann 1994; Buffle et al. 1998; Schemel et al. 2000). Indeed, natural colloids and particles display a much larger specific surface area, due to their small size. Also, because of their heterogeneous composition, of their low crystallinity, they display a high proportion of surface groups likely to bind metals, and as a consequence a higher surface reactivity. The study of such solid phases, besides global metals concentrations, requires specific methods, taking into account the high heterogeneity and the amorphous character of most of their constituents. Then, micro-scale and nano-scale information must be obtained, which calls for the use of spectro-microscopic techniques. In that context, electron microscopy (SEM, TEM, and STEM) has been extensively used (e.g., Mavrocordatos et al. 2007; Filella et al. 2009). Such techniques provide high spatial resolution and can be advantageously combined with Energy Dispersion of X-rays Spectroscopy (EDXS), which helps in the identification of poorly crystallized phases and metallic contaminants scavengers, that can not be identified by classical XRD. However, these techniques present a few drawbacks (high vacuum conditions,

beam damage, relatively high detection limits of EDXS). It is then worthwhile to combine them with X-ray based techniques such as X-ray microfluorescence (e.g., Isaure et al. 2002; McLean et al. 2011) and X-ray microscopy (TXM and STXM). This latter technique can be performed in wet conditions and provides spectroscopic information that can be spatially resolved at a sub-micronic scale (e.g. Bluhm et al. 2006; Dynes et al. 2006; Miot et al. 2009).

The present work is a case study focusing on a highly polluted river located in the North East of France, the Fensch river. Sediments and suspended particulate material (SPM) from the Moselle-Fensch junction were previously studied and displayed high concentrations in heavy metals such as Zn, Sn, Cr and Pb as well as a high iron content (Montarges-Pelletier et al. 2007). A strong correlation was evidenced from bulk analyses between iron and heavy metals contents in SPM and sediments (Zn, Cr, Pb). This correlation at macro-scale suggested that most of the heavy metals were concomitantly entering the river system. The sediments accumulated in the vicinity of the Fensch-Moselle junction were shown to integrate the contamination of the entire watershed, past and actual. In order to study the origin and fate of heavy metals in the Fensch river, sampling was extended from the source in Fontoy to the junction with Moselle in Illange. The molecular characterization of organic matter (Jeanneau et al 2008), and more specifically of the lipidic fraction had already evidenced the evolution of organic contaminants origin on the Fensch linear. The following paragraphs aim to show that iron particles and associated heavy metals are not simply transported and/or accumulated in sediments, but are also modified in terms of speciation and distribution between compartments. Thus, the presented results will focus on the distribution of heavy metals between the three compartments, i.e. dissolved fraction, SPM and sediments, as well as on the interactions between heavy metals

and suspended materials, and specifically iron-rich suspended colloidal and particulate materials. This will be achieved by combining global elemental analysis and various microspectroscopic techniques i.e. TEM-EDXS, SEM-EDXS, micro-XRF and STXM. This latter technique allows obtaining spatially resolved NEXAFS spectra at Fe $L_{2,3}$ edges that are particularly sensitive to iron valency and coordination symmetry (e.g., Rivard et al. 2013; Yoon et al. 2004; Bluhm et al. 2006; Benzerara et al. 2007). The analytical data collected at different scales, from bulk to nanometer, unraveled the influence of settling-re-suspension cycle of sediments on the fate of metals within such highly contaminated surface waters.

Experimental section

Study area

The study area is located in the downstream zone of the Moselle basin, past the main cities of the region, Nancy and Metz, upstream the border with Luxembourg and Germany, where Moselle river finally discharges within the Rhine in Koblenz. Fensch river flows through a highly industrialized valley, well-known for steel-making activities. For more than a century, this small river has been considered as a natural sewer and was then the receiving end of numerous industrial and domestic inputs. Consequently, it was classified as the most polluted river in France in the 80's. As it is one of the tributaries of the Moselle river, its contamination represents a serious threat to the quality of Moselle waters that are used as drinking water resource. Despite recent improvement in industrial wastewaters treatment, past and present industrial and domestic inputs, as well as leaching of urban surfaces maintain a high anthropogenic pressure on this hydrosystem. Furthermore, as a significant portion (> 50%) of the river is covered

by public and private facilities (Figure 1), dredging operations have been rather limited, and large amounts of highly polluted sediments remain in place, thus maintaining a significant environmental hazard. The complete geographic situation was already described in previous papers (Jeanneau et al. 2006; Montarges-Pelletier et al. 2007).

Sampling methods and elemental analysis

Figure 1 displays the different sampling sites used in the present study, Fontoy (FO), Knutange (KN), Seremange (SE), Florange (FL), Maisons-Neuves (MN) and Illange (IL). For each station, 20 liters of water were sampled for the study of suspended particulate material by immersing pre-cleaned 10 L polyethylene containers 30 cm below surface level. Conductivity, pH, turbidity and oxygen values were measured on site, with electrodes dedicated to field-measurements (Multiline F/SET, WTW) and by turbidimeter (2100P).

An aliquot of 100 mL was immediately filtered at 0.22 μm on cellulose syringe-filters, split into three distinct containers dedicated to DOC analysis, cations, and anions concentrations measurements, respectively. Samples for cations analysis were subsequently acidified with HNO_3 1 N. Samples were stored at 4°C until analysis. The resulting solution was analyzed by ICP-MS (trace elements) and by ICP-AES (major elements) (SARM, CRPG Vandoeuvre-lès- Nancy). The DOC was determined with a Dohrmann DC 190. Anions (F^-, Cl^-, NO_3^-, SO_4^{2-} et PO_4^{3-}) were measured by ion chromatography (Dionex ICS-3000).

Suspended matter was retrieved from the centrifugation at 15 000 g during 20 min of 20 L of raw water and freeze-dried. SPM could also be recovered from water filtration through pre-weighed Nucleopore Membrane (47mm diameter, 0.22 μm pore size), this fraction includes particulate matter as well as colloids.

Such an additional filtration procedure provides a quantitative evaluation of suspended solids loads within Fensch waters. The resulting filter membranes were air-dried and kept under neutral atmosphere before SEM and TEM/STEM experiments.

Superficial sediments (0-10 cm) were sampled at the different stations. For the station of Illange, sediments were cored on about 50 cm to investigate the evolution with depth, core samples were divided in three parts from the top to the bottom: 0-10 cm, 10-30 and 30-50 cm. The different sediments samples were then frozen, freeze-dried and sieved at 2 mm, 250 μm and 50 μm. The different analyses were performed mainly on the coarse and fine fractions 0-2 mm and 0-50 μm. For SPM and sediments, elemental composition was determined through ICP-MS and ICP-AES (SARM, CRPG Vandoeuvre-lès- Nancy).

Microscopic and microspectroscopic methods for solids

Electronic microscopies

For TEM (Transmission Electronic Microscopy) analysis, filter fragments were suspended in ethanol, releasing fine particles and colloids, and ultrasonicated during twenty minutes to enhance particle dispersion. One drop of the resulting suspension was put down on a Cu grid coated by a carbon membrane (EuroMEDEX, Mesh200). TEM was carried out using a CM20 Philips TEM with 200 kV accelerating voltage. The electron microscope is coupled with an EDAX EDXS. Stoichiometric ratios can then be calculated from atomic percentages given by EDX spectra, and compared with known mineralogical compositions. A spot size of about 40 nm was used to record EDX spectra with a counting time of 40 s and dead time below 25%. EDX calibration standards were run to obtain

quantitative analyses of major and trace elements with a detection limit of about 1000 ppm.

Scanning Transmission Electron Microscopy observations were performed by focusing the electron beam into a narrow spot of 5-10 nm that is scanned over the sample. The rastering of the beam across the sample is used for mapping by EDX spectroscopy. Images were recorded in bright field BF. The scan raster is 256 x 256 points with a dwell time of 30 μs per pixel. The area to be scanned is selected from a low magnification image.

For SEM (Scanning Electron Microscopy), a Hitachi 54800 Scanning Electron Microscope equipped with a Kevex 4850-S EDX was used. One filter fragment was taped with carbon-tape onto 2 cm^2 plates and carbon coated. Backscattered electron imaging (BEI) was used to locate the particles of interest. In that mode, brightness is related to the average atomic number of materials, and the mineral phases bearing heavy elements appear as bright spots that can be easily detected. In order to increase the emission of backscattered electrons, the SEM microscope was generally operated with a beam current of 3 pA and an accelerating voltage of 20 kV (analyzed micro-volume of about 6 μm^3). However, to improve the quantification of low atomic number elements, EDX analysis was sometimes carried out at an accelerating voltage of 10 kV (sampling volume of 3 μm^3).

Synchrotron based X-ray Fluorescence

Synchrotron-based X-ray fluorescence experiments were performed at beamline L in Hasylab light source facility, Hamburg, Germany. Aqueous suspensions of river material were filtered on cellulose filters that were directly analyzed by X-ray fluorescence. The monochromatic X-ray beam (15 keV) was focused on the sample using borosilicate glass polycapillaries with a resulting beam size of 10

μm. Samples were placed on a motor x,y,z stage with a movement precision of 1 μm. Maps were acquired on various zones of the filters with 10 μm step size and dwell times of 5 sec. Fluorescence spectrum on each point was collected using a Vortex-EX (Radiant Detection Technologies) Silicon Drift Detector with 50 mm^2 active area. The XRF spectra were evaluated using the AXIL software package (Falkenberg et al. 2001; Osan et al. 2004).

X-ray microscopy

STXM experiments were carried out on the PolLux beamline located at the Swiss Light Source (SLS) Paul Scherrer Institut Villigen, Switzerland (Raabe et al. 2008). The SLS storage ring runs at 2.4 GeV in "top-up" operation mode, which guarantees a constant electron beam current of 400 (±1.5 mA). The PolLux STXM beamline uses polarized X-rays from a bending magnet in the photon energy range between 200 and 1200 eV. X-ray beam is focused by a 25 nm zone plate. The lateral resolution is about 40 nm in routine operation, with a spectral resolving power ($E/\Delta E$) better than 3000 at iron $L_{2,3}$ edges, and a detected flux in helium of more than 2 x 10^6 photons/s. Raw river water (10-20 μl) was deposited between two silicon nitride windows, with a surface of 1 mm^2 and a thickness of 100 nm. The experimental protocols used for STXM data acquisition and analysis can be found elsewhere (Jacobsen et al. 2000; Hitchcock 2001; Lerotic et al. 2004). XANES spectra were obtained by performing image stacks collected by scanning the sample in x–y direction on an area of a few square microns at energy increments of 0.2 eV over Fe $L_{2,3}$-edges energy range (695–730 eV). The AXIS2000 software was used for data and image processing (http://unicorn.mcmaster.ca) (Hitchcock 2001). Images of a given stack were first aligned with each other using a correlation method and converted into optical

density (OD) according to the following equation: $OD = - \ln(I/I_0)$ where I represents the transmitted intensity at the point of interest and I_0 represents the incident intensity and was derived from empty regions in the images (no particle areas). I_0 includes the absorption by silicon nitride windows. In order to separate particles with different Fe L-edges spectrum, two procedures were tested for each stack. On one part, a manual procedure, using the sub-routine Zimbra, was used to select regions of interest. On the other part, in order to check that all the diversity of spectra and thus the diversity of iron phases was covered by the manual procedure, we applied principal component analysis (PCA) and cluster analysis (Lerotic et al. 2004; Lerotic et al. 2005). The spectra extracted using either Zimbra routine were all corrected in energy position, and a linear background was subtracted. Resulting spectra were all normalized setting their area to 1. Reference spectrum of berthierine (a silicate containing mainly Fe^{2+}) was multiplied by 0.8 as a correction factor to take into account the difference in occupancy of the 3d orbitals in Fe^{2+} and Fe^{3+} ions (Van der Laan and Kirkman 1992). Experimental spectra were fitted with linear combination of normalized reference spectra of one Fe^{2+} phase and one Fe^{3+} phase, applying the CGO (Conjugate Gradient Optimization) curve fit routine in aXis2000. The coefficients thus obtained were used to calculate Fe^{2+}:Fe^{3+} ratio in the probed zones.

Results

Field parameters and major ions in solution

Table 1 displays global parameters measured on Fensch waters for the different stations. Our data were compared to mean, maxima and minima values provided by water quality database (Water Information System Rhine-Meuse, SIERM, http://rhin-meuse.eaufrance.fr/) resulting from monthly measurements on the

2001-2011 period. For most of the parameters that were measured, the values stay in the range covered by SIERM data.

Regarding the general evolution of water chemistry along the Fesnch river, there is a strong increase of conductivity value and major ions concentrations in Knutange, the second station, followed by a slow decrease from Knutange to Illange. Conductivity values are strongly influenced by the input of mine de la Paix surcharge in Knutange, which brings sulfates, sodium, calcium, magnesium, silicium, manganese, and perharps carbonates. While those latter anions were not measured, mean values suggest an increase of their concentrations in Knutange. High concentrations in hydrogenocarbonates are linked to the carbonaceous formations of Mosellan plateau and are also responsible for relative high values of conductivity.

Suspended solids content (SS), and to a lesser extent, dissolved organic carbon concentration (DOC), display an increase in the station of Seremange, and slightly increase from Seremange to the confluence. The station of Seremange stands after a rather long covered part, downstream the industrial facilities and urban areas of Nilvange, Hayange and Seremange. NO_3, Na, K and to a lesser extent Al, slightly increase at Seremange station suggesting that anthropogenic inputs in Seremange are richer in those four elements.

From these global parameters, two stations were shown to strongly influence the chemistry of Fensch waters: Knutange due to the mine surcharge and Seremange due to the quantitative inputs of industrial and domestic waste waters.

Evolution of trace and major elements in waters, SPM and sediments along the Fensch linear

Figure 2 presents the evolution of waters concentrations and SPM and sediments contents for zinc, nickel, and chromium (plots A-C). Those three elements were

selected as they represent three distinct behaviors or three different evolution trends in Fensch waters from upstream to downstream. In order to improve the reading, evolution of concentrations for copper, lead, cobalt, arsenic and manganese were not presented (Online Resource), but will be discussed in the following paragraphs. Iron contents (provided as the percentage of Fe_2O_3 iron oxide) are also presented for SPM and surface sediments collected in the five distinct stations (Figure 2 plot D). Iron was predominantly present in the colloidal and particle fractions, and was not detected in solutions.

In waters, Zn concentrations show a striking increase at the Seremange (SE) station (Figure 2 plot A), going from 9 $\mu g.L^{-1}$ in Fontoy to 471 $\mu g.L^{-1}$ in this station. Such an increase is clearly linked to the fact that Seremange is the first sampling station located after the industrial facilities belonging to Corus-Rail in Nilvange and Arcelor-Mittal (Hayange and Seremange) (Figure 1). The measured concentrations are far above the commonly Zn concentrations encountered in the adjacent Moselle river (Montargès-Pelletier et al. 2007). The sampling campaign was performed during a rain event, that may explain the particular high Zn concentrations. The Zn concentrations for the following stations of Maisons-Neuves and Illange are slighlty lower, respectively 221 and 215 $\mu g.L^{-1}$ suggesting a dilution by supplementary inputs such as treated waste waters from the WWTP located just before Maison-Neuve station, and/or the Krisbach waters entering the Fensch river between Maison-Neuve and Illange stations.

Concerning the solids, there is a simultaneous increase of Zn SPM and sediment contents in Seremange, as the values go from 780 $mg.kg^{-1}$ to 1892 $mg.kg^{-1}$ and from 566 to 1058 $mg.kg^{-1}$ respectively. However, while Zn concentrations rather suggest a dilution phenomenon, for the last station of Illange, Zn contents reach

2765 $mg.kg^{-1}$ in sediments and 3720 $mg.kg^{-1}$ in SPM. Similar trends were observed for Cu, Mn and Pb (Online Resource).

The major ions analysis in waters previously evidenced that the Knutange Mine exhaust (KN) acts on water composition through an increase of major ions concentration (Table 1). However, as the water flow from the mine is well above the Fensch flow, it dilutes some of the elements present in Fensch waters before the mixture with mine waters. Those surcharge waters appear enriched in Ni (figure 2 plot B) as this element display an increase in water concentrations at this station (4.8 $\mu g.L^{-1}$ in Fontoy and 11.6 $\mu g.L^{-1}$ in Knutange). For the following stations, Ni concentration tends to decrease, reaching 7.2 $\mu g.L^{-1}$ in Illange. Ni contents in SPM do not present strong variations, ranging from 31 to 61 $mg.kg^{-1}$, and the maximum value occurs in Seremange and not in Illange as it was the case for Zn. As far as sediments are concerned, Ni contents increase regularly along the Fensch linear and the maximal value is measured in sediments from the last station, Illange. A similar trend was observed for cobalt (Online Resource).

The third plot (Figure 2 plot C) displays the evolution of Cr concentrations and contents in waters, SPM and sediments respectively. Cr concentrations regularly increase from Fontoy to Illange with a maximum value of 6.6 $\mu g.L^{-1}$ in Illange. For Cr, the SPM and sediments contents display the same evolution as waters concentrations and Cr contents in Illange reach 267 and 693 $mg.kg^{-1}$ in SPM and sediments respectively. A similar trend was observed for As (Online Resource).

In the case of iron (Figure 2 plot D), contents are given as percentage of iron oxide Fe_2O_3. Fe_2O_3 in SPM increases downstream, with an edge in Seremange at 7.9 %. There is an increase of iron-rich particles inputs from several industrial facilities between Nilvange and the exit of this small watershed, and sediments show similar evolution of iron contents. The X-ray diffractograms of sediments

along (Online Resource), confirm the increasing presence of iron-phases. Besides classic sedimentary mineral phases (quartz, calcite, dolomite and feldspars), magnetite Fe_2O_3, hematite Fe_3O_4, wuestite FeO are encountered, iron oxides being the predominant iron phases detected through XRD.

Despite the fact that iron was not detected in solution, it can be compared to Cr as for both elements, SPM and sediments contents increase, and Cr and Fe contents in sediments are higher than in SPM.

Iron, heavy metals and metalloids (Zn, Ni, Pb, Cu, Co As) contents in sediments are definitely higher in Illange. Actually, the last section of the Fensch river, meaning about one kilometer before the Moselle river, is a stagnant reach, with a over-calibrated and uniform river bed, surrounded by imposing banks. This last section is then an accumulation zone for solid materials coming from the entire watershed (Montargès-Pelletier et al. 2007, Jeanneau et al. 2006, 2008). Although Illange sediments appear as a metallic contamination sink, detected metals do not display similar evolutions along the Fensch linear and are heterogeneously distributed among the three investigated compartments. This heterogeneity can be explain not only by the origin variations of metallic contamination, but also by the variation of chemical speciation and association mode with suspended particles.

Status of Iron in suspended particles: microanalyses using SEM, TEM and STXM

The comparison of heavy metals and iron contents in the dissolved, particulate, sediment fractions strongly suggest the association of heavy metals with iron-bearing colloids and particles. This could be further analyzed by focusing on four stations: Fontoy, Seremange, Maison-Neuve and Illange. Fontoy is close to the source of the Fensch and should be the least affected by industrial or domestic

discharge although previous works evidenced the presence of human waste markers at this point (Jeanneau et al. 2006). The station of Seremange is the first easily accessible station located in a heavily industrialized area, downstream two steel manufacturing and making plants (Corus-Rail and Arcelor-Mittal). Maisons-Neuves and Illange are located downstream. Furthermore, the high iron contents in SPM and sediments call for a better knowledge of iron bearing phases in those matrices. It is then of prime interest to analyze if the modifications of heavy metals partitioning occurring along the Fensch river is linked to changes in the status and speciation of iron-bearing suspended materials.

Because XRD only evidenced the presence of crystalline phases, it was mandatory to carry out spatially resolved investigations on SPM samples, in order to get a more precise picture of the mineralogy of iron particles and, as a consequence, a better idea of their ability to trap and transport heavy metals within the Fensch waters. Such microanalyses also provide the nature of metal carriers.

Fontoy

Figure 3A displays a general SEM view of SPM from Fontoy. The most obvious feature is the presence of numerous diatoms of various shapes and sizes. Diatoms are commonly encountered in fresh waters, and particularly in the spring. They are often used as biological indicators of the water quality, and particularly rivers eutrophication (Kelly and Whitton 1995). Although the presence of diatoms should be expected in continental streams, the observation of such biological organisms in the station of Fontoy provides a general indication of water quality. Actually, no more diatoms, or scarcely only, could be observed for the following stations. A closest view (Figure 3B) reveals mineral aggregates, which, on the

basis of EDXS analysis, were shown to be constituted of numerous sub-micrometric phyllosilicates (that were identified to illites and interlayered illite/smectite), quartz, feldspars and calcite grains, covered by parts of silica diatoms skeletons. Scarce bright spots were assigned to iron oxihydroxide particles.

Figure 3 presents two STEM micrographs (C and D). Associated elemental maps and EDXS spectra (Online Resource) confirm that the main mineral phases are phyllosilicates and carbonates with a few phosphate phases. A nanometric spherical mineral can be noticed on the left micrograph (red arrow on Figure 3C), made essentially of calcium and phosphorus. This mineral was identified as apatite, a calcium phosphate commonly encountered in urban waters (Houhou 2009). Iron is mainly present in clay layers. The microanalysis carried out on Fontoy SPM revealed a rather classical composition as expected for suspended solids from continental rivers.

Seremange

Particles collected at Seremange station are strikingly different from those observed in Fontoy. Figure 4A presents a SEM micrograph, collected in backscattered electrons mode. Large iron-rich plates are encountered, and numerous bright points can be observed, revealing a strong increase in high atomic number elements. EDXS analysis on these different electron scattering zones demonstrated the high contents in iron. Using higher magnification, spherical (Figure 4C) or star-like (Figure 4B) iron-rich particles are observed. The Fe/O ratios in these particles vary between 0.5 and 0.9, which indicates the presence of various iron or iron-mixture phases with compositions evolving from oxihydroxides (ferrihydrite, goethite $FeOOH.nH_2O$, Fe/O = 0.5-0.4) to oxides

(hematite or maghemite Fe_2O_3 (Fe/O = 0.66), magnetite Fe_3O_4 (Fe/O = 0.75) or wuestite FeO (Fe/O=1)). Among the various morphologies of iron-rich phases, spheres are the most frequently encountered with sizes ranging between 10 nm and a few microns, displaying atomic ratios Fe/O between 0.66 and 0.75. Such ratios suggest a mixture of magnetite and hematite spherical particles. Due to the superimposition of several entities, good conditions for electron diffraction were never reached, and the mineralogical identification of those spherical particles was resolved on the basis of elemental analyses with EDXS. XRD data (Online Resource) for Seremange SPM confirmed the presence of both magnetite and hematite with rather close occurences.

To investigate SPM constituents at a submicrometric scale, TEM and STEM micrographs were obtained for Seremange particles (Figure 4 D & E). As in the SEM images, spherical particles (black in that case) are easily detected. In contrast with what was observed in Fontoy, iron is present as the main constituent of numerous particles, detected for 88% of investigated particles, with Fe percents ranging from 0.2 to 49 % (50 % of iron-bearing particles display Fe percent above 20%). EDXS analysis of individual iron particles evidence Fe/O atomic ratios ranging from 1 to 0.6, with a mean value at 0.75 suggesting the predominance of wuestite, magnetite and hematite particles. For such particle, electron beam was hardly transmitted and was set at the edge of the particle to favor the detection of oxygen fluorescence photons, that tend to be re-absorbed by iron rich spherical particles.

Figure 5 presents typical STXM images obtained on particles collected at Seremange. The presence of iron rich particles (black spots) is evidenced through the division of high resolution images respectively collected before iron edge and at iron edge (Figure 5A). A stack of images was then collected on a reduced zone

(red square), from which spectroscopic data could be extracted at the pixel scale (50 nm). PCA routine was run for this Seremange stack, in order to rise up the different spectra. However, the results were influenced by the presence of thick iron particles. In order to reveal the diversity of iron phases, manual definition of regions of interests (ROIs) was preferred. The resulting ROIs are shown on Figure 5B (dashed lines), and associated Fe $L_{2,3}$ edge spectra on figure 5D. Reference spectra are displayed on Figure 5C, to compare sample spectra with those obtained on various iron-bearing reference minerals. For ferric and ferrous iron, Fe $L_{2,3}$ edges can be primary described as transitions from a ground state Fe $2p^63d^5$($2p^63d^6$) to a final excited state Fe $2p^53d^6$ ($2p^53d^7$) respectively. Calculated spectra based on the nearly atomic transition of these configurations have shown different fine structures for these two valence states (van der Laan and Kirkman 1994). In the case of the 4 standard minerals used here, the oxidation state of iron strongly affects the spectral features of the different samples. This is particularly marked by the presence of a signal at 708 eV that is clearly much more intense for Fe^{2+} bearing minerals (Berthierine and Magnetite, bottom curves on Figure 5C). L_2 peaks also display slight modifications in the relative intensities of major contributions at 722.5 and 724 eV. In the case of Berthierine (that can extrapolated to Fe^{2+} oxide), the low energy component of L_2 edge increases in intensity while the high energy component decreases. A supplementary signal at 720 eV also indicates the presence of ferrous iron. This peak is absent in both maghemite and ferrihydrite (top curves).

Each ROI spectrum was fitted as a linear combination of ferrous and ferric iron mineral phases, providing Fe^{3+} percentage. On the basis of these linear combination fittings, Seremange spectra could be classified in two main groups. One first group evidences the presence of ferrihydrite-like phases, while the

second group evidences the presence of mixed valence oxides with Fe^{3+} percentage going from 49 to 70%. SPM collected at Seremange then clearly display significant amount of Fe^{2+} bearing phases. This result goes well with Fe:O ratios obtained from TEM and STEM investigations, and supports the hypothesis of mixture of different oxides going from pure Fe^{2+} wuestite or FeO to pure Fe^{3+} Fe_2O_3 or $FeOOH.nH_2O$.

The occurrence of iron oxides with relative high contents in ferrous iron may be linked to the location of that sampling station, just downstream the first set of steel-making facilities (high furnaces) and just at the exit of the longest covered section of the Fensch river (3 km). The low oxygen content in water at this location confirms the reductive conditions. Still, it must be pointed out that according to literature data (Todd et al. 2003) none of the collected spectra corresponds to iron sulfides.

Maisons-Neuves (MN)

Figure 6 presents some SEM and TEM observations of SPM collected at Maisons-Neuves. The general view displayed in Figure 6A exhibits features similar to those observed in Seremange with frequent iron-bearing particles. At higher magnification, numerous eroded spherical particles are observed. Iron rich filamentous structures that were not observed in Seremange are also encountered (Micrographs C and D). The atomic ratio Fe:O tend to decrease slightly, several iron rich particles show Fe/O atomic ratio corresponding to oxyhydroxides (close to 0.5) and the occurrence of spherical iron oxides is reduced. Instead, heterogenous particles and aggregates of particles are ubiquitous, combining iron oxides and oxyhydroxides, phosphates, carbonates, aluminosilicates and sulfides.

Zn could be detected for 75% of studied points, with atomic percentage ranging between 0.2 and 27%.

A typical STXM image of SPM collected at Maisons-Neuves is presented in Figure 7. In that case, PCA routine was carried out to evidence the distinct spectra. In contrast with what was observed in Seremange (Figures 4 and 5) Fe^{2+} rich particles are very scarce (small blue particle in Figure 7 C, spectrum on Figure 7D). It must also be noticed that numerous bacteria are systematically observed on all the images. This can be directly related to the direct input of untreated domestic waste waters and/or to the presence just upstream of this collection point of a wastewater treatment facility using a biological activated sludge process. The role of these bacteria and of the associated Natural Organic Matter (NOM) in the increased mineralogical modifications of iron rich materials is likely, although no direct evidence for such processes can be provided.

Illange (ILL)

TEM micrographs of SPM from Illange are shown in Figure 8. The amount of iron-rich filamentous structures is even higher than what was observed in Maisons-Neuves. EDXS analyses reveal that these structures are rich in iron and in heavy metals, essentially Zn, occasionnally Pb. The Fe:O ratio in these filaments is relatively low, around 0.5-0.4 which indicates not only a more oxidized status, but also the predominance of ferrihydrite-like materials or amorphous Fe-oxyhydroxide. Such filamentous or hairy particles are often combined with calcium phosphates and aluminosilicates (clay minerals). The EDX spectrum shown on Figure 8-B1 represents about 68 % of investigated particles with TEM-EDXS.

Figure 9 presents one of the stacks acquired for SPM from Illange. Those STXM experiments confirm the morphological changes evidenced by TEM. Indeed, aggregates appear less dense and present a common filamentous character. The stack analysis could not evidence more than one single iron status, presented on Figure 9-C. This spectrum, using linear combination fitting, was assigned to ferric oxyhydroxide. Then, STXM data confirm more pronounced changes in oxidation state and iron mineralogy. All spectra measured on Illange particles are close to those of Fe^{3+} oxyhydroxides and no Fe^{2+} bearing particles was ever observed for SPM from this location. Morphology strongly suggests the predominance of oxyhydroxides.

Status of metals (Zn) in suspended materials: synchrotron-based microfluorescence and TEM-EDXS

X-ray fluorescence maps were acquired for SPM collected in Illange and several zones of about 640 microns per 700 microns were investigated using a 10 μm micro-beam at 15 kV. In order to approach the links between iron-rich particles and trace metals, elemental maps were built on the basis of their emission lines intensity. Furthermore, resulting maps representing the spatial distribution of Ca, Fe, Zn, Pb and Cu were treated point by point to yield correlation graphs, to which linear regression was applied (Figure 10 and Table 2). Ca was used as a "witness-element", its abundance in the sample was sufficiently high so that it could be readily detected.

Figure 10 presents Fe and Zn distribution zones obtained for two distinct zones on Illange SPM sample. For the first one (Zone 1, top of the figure) Fe and Zn appear strongly correlated while for the other one those two elements are weakly correlated. Thus, the distribution map obtained for Zone 8 display independent

Zn-rich spots and Fe-rich spots. Table 2 provides correlation factors calculated from linear regressions on nine different zones, inclunding the zones 1 and 8. At first glance, these numbers tend to evidence the strong heterogeneity of the sample and traduce the rather weak spatial correlation between metals and Fe, at the scale of this micro-XRF investigation, i.e. 10 microns. Indeed, correlation factors rarely exceed 0.5. These numbers are strongly influenced by the presence or not of independent metal-rich spots and Fe-rich spots, and a kind of relation appears between those correlation factors and Fe K_{α} counting. Indeed, the zones with relatively low iron particles, showing low Fe couting, tend to give the highest correlation factors (Table 2), showing that the presence of pure Fe-oxides modify the correlation.

For the other elements than Zn, i.e., Pb, Cu, the results were more difficult to analyze due to their lower abundance in the sample. Indeed, the distribution of those elements and the resulting correlation factors with iron-rich particles was strongly influenced by the presence of few Cu/Pb hotspots, those hot-spots being iron free or with a rather low iron content. These microfluorescence maps suggest then that Zn, Cu, Pb are present with at least two different status, the commonest one being related to iron-rich particles, the second one related to iron-free particles or iron-poor particles.

TEM and STEM analyses were also carried out to detect the occurrence of trace elements by EDXS. However, due to the relative high level of detection, i.e. 0.1%, Zn could be detected for a sufficient number of particles, and Cr and Pb were only occasionally detected.

For Fontoy, trace elements are almost all below the detection limit of EDXS except for Zn that is evidenced at relatively low concentrations for few particles (0.1-0.5%). For Seremange SPM sample, Zn was detected for about 65% of

investigated particles, while Pb and Cr were rarely detected, and about 6% of particles display Pb in their elemental composition. Atomic percents of Zn range between 0.2% and 46%, and particles with Zn content below 1% represents 75% of the particles displaying Zn. Morevover, half of the particles for which Pb was detected are the particles with the highest Zn atomic percent. As far as Zn is concerned, its occurrence is particularly correlated to that of iron, as shown by STEM –EDXS elemental maps (Figure 4 D & E). Zn is occurring with different kinds of particles or aggregates of particles, from the most prevalent to the rarest, (i) Zn associated to iron oxides, (ii) Zn associated to heterogeneous aggregates essentially constituted of iron oxyhydroxides, aluminosilicates (clays), phosphates and carbonates, (iii) Zn sulfides. Those three kinds of Zn-bearing particles are sorted from the Zn-poorest to the Zn-richest.

For the following stations, Maison-Neuve and Illange, Zn could be detected for 75% and 76% of studied points respectively, with atomic percentage ranging between 0.2 and 27% for Maison-Neuve and between 0.2 and 25% for Illange. The nature of Zn carriers are qualitatively similar to those encountered in Seremange (Figure 9), but Zn was never more occurring as being associated to iron oxides. Zn-sulfides (Figure 9D) particles represent 4% or analyzed particles in Illange, and thus are far less encountered than Zn-bearing aggregates (Figure 9 A and B). Moreover, in Illange, SPM display Zn-bearing particles with no presence of iron or relatively low presence of iron (figure 9 micrograph C, 5% of investigated particles). Such particles, presenting a fibrous shape, are constituted of aluminum oxyhydroxides and calcium phosphates and Zn was detected with atomic ratio ranging between 3 and 6%.

Discussion

Along the Fensch river, the evolution of metals concentrations in solution is not identical for all metals (Figure 2 and Online resource). The elemental analyses on SPM and sediments tend to evidence an enrichment of SPM in Cu, Zn, Mn, Pb towards water and surface sediments for the last station on the Fensch linear, in the vicinity of the junction with the Moselle river. The variation of SPM content, of DOC which both tend to increase from upstream to downstream are not sufficient to explain the evolution of partitioning, and the modification of SPM composition might be retained as a possible explanation (Shäfer et al 1997). This metallic enrichment of SPM is apparently associated with the evolution of iron status in SPM, for which a global increase in oxidation state along the Fensch linear was revealed by SEM, TEM (Fe:O atomic ratio) and STXM. The evolution of iron oxidation state in SPM is combined to intense mineralogical modifications leading to significant morphological changes (Figures 6-9). Various mechanisms can explain the observed evolution. First of all, due to their high density, anthropogenic iron oxide particles such as those observed at Seremange station (Figure 4), tend to settle as shown by XRD patterns from sediments (Online resource). Although it was not specifically studied in this work, it is now admitted that biotic and abiotic oxidation processes occur at the water-sediment interface (Santschi et al. 1990, Warren and Haack 2001). Fensch waters and Fensch sediments are relatively rich in domestic organic matter (Jeanneau et al 2006, 2008), and it can be readily suggested that a relatively high biotic activity stands in the first layers of sediments. The abundance of microbes in the Fensch waters is evident and undoubtedly provokes the iron oxidation and mineralogical transformation. Indeed, as iron is used as electron donor for specific bacterial

metabolisms (Fortin and Langley 2005, Mitsunobu et al. 2012), its cycle is commonly associated with microbial activity. In the case of the Fensch river, the oxidation processes of mineral particles should be prevented due to the relative high amount of organic matter which constitutes an O_2 "consumer" for its own decomposition. Furthermore, opulent organic matter may also act itself as a major factor of iron-particles modification. First, iron readily forms stable complexes with organic matter (Stumm and Morgan 1996, Rose et al. 1998), and the relatively high concentration in dissolved organic carbon (DOC, see table 1 and figure 11) could influence the iron oxides dissolution. Secondly, organic matter certainly recovers the surface of iron particles when released in the aqueous medium, and participates then to the general processus of dissolution-reprecipitation. The organic coating of particles was already reported for sediments in a previous paper, with the use of FTIR in reflectance mode (Montarges-Pelletier et al 2007).

For a upstream-dowmstream trend, settling and biochemical modifications resulted not only in an increased occurrence in sediments of iron oxides such as magnetite, wuestite, and hematite but also in the apparition of hetereogeneous aggregates composed of hairy iron oxyhydroxides. The mineralogical modifications may occur at different locations : in the water column, or in the upper levels of sediments and due to the relatively weak depth of Fensch river (inferior to 1 m), the latter is certainly more efficient. However, the chronicity, the kinetics of weathering processes is difficult to precise and due to frequent remobilization phenomena of Fensch sediments, the cycle of Fensch SPM is not straightforward to describe. Furthermore, the fact that Illange sediments show relatively high contents in Fe^{2+} bearing oxides (wuestite, magnetite) can also be a result of a selective remobilization of iron particles, enhancing the re-suspension

of hairy and low-density oxyhydroxides. The succession of these three steps of settling, intense weathering and resuspension is the main explanation for the above described evolution of iron status in SPMs along the Fensch linear. This assumption was reported on a graphical summary (Figure 11).

Although organic matter was commonly reported as metal-scavenger in natural waters (e.g. Buffle et al 1977, Logan et al 1997, Murphy and Zachara 1995, Dupré et al 1999), the abundance of iron particles in the Fensch waters tends to minimize the role of organic matter in terms of metal sorbents. The iron cycle in Fensch waters certainly influences the fate of metals, and certainly in a predominant way. The mineralogical modifications of iron particles may have direct consequences on the amount of heavy metals present in SPMs through two associated mechanisms. First, the formation of filamentous structures increases the specific surface area available for ion adsorption. These enhanced surface properties may explain also why such iron oxyhydroxides are associated with carbonates and phosphates phases. Second, newly formed iron oxy-hydroxides are efficient scavengers of heavy metals as shown in numerous studies (e.g. Tessier et al. 1985; Honeyman and Santschi 1988; Schwertmann and Taylor, 1989; Warren and Hack 2001; Waychunas et al. 2005).

Cr, Ni and Zn were selected to describe three distinct evolution trends in the Fensch waters. Chromium is supposed to be chemically bound to iron oxides as the trend of its contents (except in solution) follows iron content in SPM and sediments, but direct evidence could not be provided with the undertaken analytical procedure.

The Zn behaviour in Fensch waters could be precised. Microanalyses (micro-XRF and TEM-EDXS) evidence three different status for Zn in particulate fraction, including amorphous Zn-sulfides (Priadi et al 2012), and Zn associated to iron-

rich aggregates. While we could not directly evidence the chemical association mode between Zn and those complex particles, the resuspension of those iron-rich particles might be one key to explain the increase of Zn concentration in SPM (Figures 2 and 11). From the ICP-MS analyses on waters, SPM and sediments (Figure 2 and online resource), we had supposed that Mn, Cu and Pb were following the same trend as Zn. Those elements could be detected only occasionnally and the number of particles bearing Cu or Pb is not sufficient to adress some hypothesis on the nature of the bearing phases.

Thus, although SEM, TEM, STXM, micro-XRF and associated spectroscopies were shown to be provide helpful information, their use is strongly dependent on the heavy metals concentration in solid phases. While we could propose a schema for Zn fate and partitioning within the Fensch rivers, it was difficult to rise some conclusions for the other metals such as Pb, Cu or Cr.

The potential hazard that these heavy metals associated to iron-rich SPM will represent after the confluence with the Moselle river strongly depends on their mode of association. Various scenarios can be proposed: (i) outer sphere complex adsorption on iron oxy-hydroxides; (ii) inner-sphere complexes; (iii) co-precipitation of mixed mineral phases (Stumm 1993). The first case could represent a significant environmental threat as, with evolving physico-chemical conditions, weakly adsorbed heavy metals could be released in solution through dilution and/or ion exchange. Discriminating between these various cases could be achieved by following the speciation of heavy metals in SPMs before and after the confluence using (micro)spectroscopic techniques such as Extended X-ray Absorption Fine Structure. Such a study will be the object of a future publication.

CONCLUSION

The previous paragraphs dealt with the study of a highly contaminated river flowing through steel making facilities and associated dense urban areas. Besides the measurement of metals and major elements in three compartments : suspended particulate, sediments and water (< 0.22 μm), a detailed description of suspended particulate was provided through a quite wide panel of microanalytical tools, including synchrotron based techniques. Microanalyses provided crucial information about SPM composition that could not be found elsewhere, through bulk techniques such as XRD. The mineralogical and textural modifications of iron-rich suspended particles along the Fensch linear were correlated with the variations of metals content, in particular Zn, within sediments, SPM and waters. The comparison of SPM and sediments composition strongly suggest the modifications being due to a three step process (settling-weathering-resuspension). Such an assumption should be more precisely tested throught the study of iron and zinc speciation at a bulk scale.

Acknowledgements

The authors greatly acknowledge the EU for funding their travel to HASYLAB and SLS facilities through the FP7 ELISA (Transnational Access Project). We also thank synchrotron facilities HASYLAB, SLS for providing beam time on L and PolLux beamlines respectively. PolLux beamline is funded by the BMBF. This work was financially supported by CNRS-INSU (ECODYN program) and Region Lorraine through the Research network Zone Atelier Moselle. A special thanks goes to Francis Borghesi from NANCIE who set up the laboratory van before each sampling campaign, and to Ali FALL from CAVF (Fensch Valley Cities Community), for selecting and providing access to the different stations. The authors also acknowledge Benjamin WATTS and Jorge RAABE from PolLux beamline for the technical support.

References

Benzerara K, Menguy N, Banerjee NR, Tyliszczak T, Brown GE Jr, Guyot F (2007) Alteration of submarine basaltic glass from the Ontong Java Plateau: a STXM and TEM study. Earth Planet Sci Lett 260:187-200.

Bluhm H et al (2006) Soft X-ray microscopy and spectroscopy at the molecular environmental science beamline at the Advanced Light Source. J Electron Spectrosc Relat Phenom 150:86-104.

Buffle J, Greter FL, Werner H (1977) Measurement of complexation properties of humic and fulvic acids in natural waters with lead and copper ion-selective electrodes. Anal Chem 49:216-222.

Buffle J, Wilkinson KJ, Stoll S, Filella M and Zhang J (1998) A generalized description of aquatic colloidal interactions: the three-colloidal component approach. Environ Sci Technol 32:2887-2899.

Dynes JJ, Tyliszczak T, Araki T, Lawrence JR, Swerhone DW, Leppard G, Hitchcock AP (2006) Speciation and quantitative mapping of metal species in microbial biofilms using scanning transmission X-ray microscopy. Environ Sci Techno. 40:1556-1565.

Falkenberg G, Clauss O, Swiderski A, Tschentscher T (2001) Upgrade of the x-ray fluorescence beamline at HASYLAB/DESY. X-ray Spectrom 30:170-173.

Filella M, Chanudet V, Philippo S and Quentel F (2009) Particle size and mineralogical composition of inorganic colloids in waters draining the adit of an abandoned mine, Goesdorf, Luxembourg. Appl Geochem 24:52-61.

Fortin D and Langely S (2005) Formation and occurrence of biogenic iron-rich minerals. Earth Sci Rev 72:1-19.

Hitchcock A (2001) Chemical mapping with soft X-ray spectromicroscopy. Amer Lab 33:30-36.

Honeyman BD and Santschi PH (1988) Metals in aquatic systems. Environ Sci Techno 22:862-871.

Houhou J, Lartiges BS, Hofmann A, Frappier G, Ghanbaja J and Temgoua A (2009) - Phosphate dynamics in an urban sewer: a case study of Nancy, France. Wat Res, 43:1088-1100

Isaure MP, Laboudigue A, Manceau A, Sarret G, Tiffreau C, Trocellier P, Lamble G, Hazemann JL, Chateignier D (2002) Quantitative Zn speciation in a contaminated dredged sediment by μ-PIXE, μ-SXRF, EXAFS spectroscopy and principal component analysis. Geochim Cosmochim Acta 66:1549-1567.

Jacobsen C, Wirick S, Flynn G and Zimba C (2000) Soft X-ray spectroscopy from image sequences with sub-100nm spatial resolution. J Microsc 197:173-184.

Jeanneau L, Faure P, Montarges-Pelletier E (2008) Evolution of the source apportionment of the lipidic fraction from sediments along the Fensch river, France: A multimolecular approach. Sci Tot Environ 398:96-106.

Jeanneau L, Faure P, Montarges-Pelletier E, Ramelli M (2006) Impact of a highly contaminated river on a more important hydrologic system: changes in organic markers. Sci Total Environ 372:183–192.

Kelly MG and Whitton BA (1995) Trophic diatom index – a new index for monitoring eutrophication in rivers. Journal of Applied Phycology 7, 4:433-444.
Lerotic M, Jacobsen C, Gillow JB, Francis AJ, Wirick S, Vogt S, Maser J (2005) Cluster analysis in soft X-ray spectromicroscopy: Finding the patterns in complex specimens. J Electron Spectrosc Relat Phenom 144–147:1137–1143.
Lerotic M, Jacobsen C, Schäfer T, Vogt S (2004) Cluster analysis of soft X-ray microspectroscopy data. Ultramicrosc 100:35-57.
Logan EM, Pulford ID, Cook GT, MacKenzie AB (1997) Complexation of Cu2+ and Pb2+ by peat and humic acid. Eur J Soil Sci 48:685-696.
Mavrocordatos D, Perret D, Leppard GG (2007) Characterisation of colloids by electron microscopy, in: Wilkinson KJ and Lead JR (eds.) Environmental Colloids and Particles: Behaviour, Separation and Characterization, IUPAC series on Analytical and Physical Chemistry of Environmental systems, volume 10, Buffle J and van Leeuwen P series eds., John Wiley and sons, pp 58-76.
McCarthy JF and Zachara JM (1989) Subsurface transport of contaminants. Environ Sci Technol 23(5):496-502.
McLean LCW, Beauchemin S, Rasmussen PE (2011) Lead speciation in House Dust from Canadian Urban homes using EXAFS, microXRF and microXRD. Environ Sci Technol 45:5491-5497.
Miot J, Benzerara K, Morin G, Kappler A, Bernard S, Obst M, Galvez M, Brown GE Jr, Guyot F (2009) Iron biomineralization by anaerobic neutrophilic iron-oxidizing bacteria. Geochim Cosmochim Acta 73:696-711.
Mitsunobu S, Shiraishi F, Makita H, Orcutt BN, Kikuchi S, Jorgensen BB, Takahashi Y (2012) Bacteriogenic Fe(III) (oxyhydr)oxides characterized by synchrotron microprobe coupled with spatially resolved phylogenetic analysis. Environ Sci Technol 46:3304-3311.
Montarges-Pelletier E, Jeanneau L, Faure P, Bihannic I, Barres O, Lartiges B (2007) The junction of Fensch and Moselle rivers, France; mineralogy and composition of river materials. Environ Geol 53: 85-102.
Murphy EM, Zachara JM (1995) The role of sorbed humic substances on the distribution of oranic and inorganic contaminants in groundwater. Geoderma 67: 103-124.
Olivié-Lauquet G, Allard T, Benedetti M, Muller JP (1999) Chemical distribution of trivalent iron in riverine material from a tropical ecosystem: a quantitative EPR study. Wat Res 33:2726-2734.
Osan J, Török S, Alföldy B, Falkenberg G (2004) Characterization of anthropogenic sediment particles after a transboundary water pollution of river Tisza using synchrotron radiation. Spectrochim Acta B 59:701-708.Priadi C, Le Pape P, Morin G, Ayrault S, Maillot F, Juillot F, Hochreutener R, Llorens I, Testemale D, Proux O, Brown G Jr (2012) X-ray Absorption Fine Structure Evidence for Amorphous Zinc Sulfide as a Major Zinc Species in Suspended Matter from the Seine River Downstream of Paris, Ile-de-France, France. Environ Sci Technol 46:3712-3720.

Raabe J, Tzvetkov G, Flechsig U, Boge M, Jaggi A, Sarafimov B, Vernooij MGC, Huthwelker T, Ade H, Kilcoyne D, Tyliszczak T, Fink RH, Quitmann C (2008) PolLux: A new facility for soft x-ray spectromicroscopy at the Swiss Light Source. Rev Sci Instrum 79: 113704.
Rivard C, Montarges-Pelletier E, Vantelon D, Pelletier M, Karunakaran C, Michot L, Villieras F, Michau N (2013) Combination Of Multi-Scales And Multi-Edges X-Ray Spectroscopies For The Investigation Of Kaolinite And Metallic Iron Interaction Products (Anoxic Conditions, 90°C). Phys Chem Miner 40:115-132.
Rose J, Vilge A, Olivie-Lauquet G, Masion A, Frechou C, Bottero JY (1998) Iron speciation in natural organic matter colloids. Coll Surf A: Physicochem Engineer Aspects 136:11-19.
Santschi P, Höhener P, Benoit G, Buchholtz-ten Brink M (1990) Chemical processes at the sediment-water interface. Mar Chem 30:269-315
Schwertmann U and Taylor (1989) RM Iron oxides in: Dixon JB and Weed SB (eds) Minerals in Soil Environments, vol. 1 (eds.), 2nd ed,. SSSA Book Ser, Madison, WI, pp 379–438
Shäfer MM, Overdier JT, Hurley JP, Armstrong D, Webb D (1997) The influence of dissolved organic, suspended particulates, and hydrology on the concentration, partitioning and variability of trace metals in two contrasting Wisconsin watersheds (USA). Chem Geol 136:71-97.
Stumm W (1993) Aquatic colloids as chemical reactants: surface structure and reactivity. Coll Surf A 73:1-18.
Stumm W and Morgan JJ (1996) Aquatic chemistry: chemical equilibria and rates in natural waters, 3rd edition, eds JL Schnoor and A Zehnder, a Wiley Interscience Publication, John Wiley &Sons, New York, 1022 p
Tessier A, Rapin F, Carnigan R (1985) Trace metals in oxic lake sediments: possible adsorption onto iron oxyhydroxides. Geochim Cosmochim Acta 49:183–194.
Todd EC, Sherman DM and Purton JA (2003) Surface oxidation of chalcopyrite ($CuFeS_2$) under ambient atmospheric and aqueous (pH 2-10) conditions: Cu, Fe L- and O K-edge X ray spectroscopy. Geochim Cosmochim Acta 67:2137-2146.
van der Laan G and Kirkman IW (1992) The 2p absorption spectra of 3d transition metal compounds in tetrahedral and octahedral symmetry. J Phys Condens Matter 4:4189-4205.
Warren LA and Haack EA (2001) Biogeochemical controls on metal behaviour in freshwater environments. Earth Sci Rev 54:261-320.
Warren LA and Zimmermann AP (1994) Suspended particle grain size dynamics and their implications for trace metal sorption in the Don river. Aquat Sci 56(4):348-362.
Waychunas GA, Kim CS, Banfield JF (2005) Nanoparticulate Iron Oxide Minerals in Soils and Sediments: Unique Properties and Contaminant Scavenging Mechanisms. J Nanoparticle Res 7:409-433
Yoon TH, Johnson SB, Benzerara K, Doyle CS, Tyliszczak T, Shuh DK, Brown GE Jr (2004) In Situ Characterization of Aluminum-Containing Mineral-Microorganism Aqueous Suspensions Using Scanning Transmission X-ray Microscopy. Langmuir 20:10361-10366.

Fig.1: Presentation of the study site. Fensch river takes its source in Fontoy and joins the Moselle river in Illange. Sampling stations are Fontoy FO, Knutange KN, Seremange SE, Maisons-Neuves MN, and Illange IL. The schematic map also presents the three tributaries Petite Fensch, Marspich and Kribsbach, the covered parts along the Fensch linear and the increase of industrial occupancy of surfaces from upstream to downstream. WWTP is located few dozens of meters before the sampling point MN.

Fig.2: Evolution of iron and heavy metal contents in waters (<0.22 μm), SPM and sediments from Fontoy (upstream) to Illange (downstream). A: Zn, B: Ni, C: Cr, D: Fe_2O_3. For A to C plots, left axis displays waters concentrations in $\mu g.L^{-1}$, and right axis displays solid contents for trace metals (in $mg.kg^{-1}$) or for iron (Fe_2O_3 %). White columns correspond to waters concentrations, grey columns to SPM contents and filled columns to sediments contents. Iron was not detected in all collected waters, the detection level being 0.03 $mg.L^{-1}$.

Fig.3: SEM micrographs in backscattered electrons mode, from Fontoy SPM. A: general view (scale bar 300 μm). B: mineral aggregate (scale bar: 30 μm). TEM micrographs (C and D). A part of diatom skeleton can be observed on micrograph C, the red arrows points a calcium phosphate bullet.

Fig.4: Seremange SPM, electron microscopies observations. A, B and C: SEM micrographs of iron-bearing particles collected in Fensch waters at the Seremange station, in backscattered electrons mode. From the left to the right: general view with a bright iron plate , a detailed view of star-like and spherical iron oxide. D and E: STEM micrographs with associated Zn and Fe elemental maps.

Fig.5: STXM data for Seremange SPM. A: Iron-rich particles map (scale bar 5 μm) obtained from the division of high resolution images collected respectively before and at Fe L_3-edge (700 and 710 eV); B and C: regions of interest and corresponding Fe $L_{2,3}$ edges XANES spectra (solid lines). Each spectrum area is normalized to 1, linear combinations fits (dashed lines) of normalized spectra of Fe^{2+} reference and Fe^{3+} reference yield the ferric iron percentages. D: Fe $L_{2,3}$ spectra for standards Berthierine (Fe^{II}-phyllosilicate); Magnetite, $Fe^{2+}Fe^{3+}{}_2O_4$; Maghemite $Fe^{3+}{}_2O_3$; Ferrihydrite $FeOOH.nH_2O$.

Fig.6: SEM and TEM micrographs of Maison-Neuve SPM. A: general SEM view displaying iron plate and heterogeneous aggregate (scale bar 30 μm), few diatoms skeletons could be noticed on this general view; B: Spherical aggregates of iron nanoparticles (scale bar 10 μm); C, D: TEM micrographs of iron-rich aggregates displaying spherical iron oxides as well as iron oxyhydroxides with hairy texture.

Fig.7: STXM treatment of Maison-Neuve SPM. A: High resolution Fe $L_{2,3}$ transmission image acquired at 710 eV. B: Iron-rich particles map (scale bar 2 μm) obtained from the division of high resolution images collected respectively before and at Fe L_3-edge (705 and 710 eV). Regions of Interest are marked with colored dashed lines. C : Fe $L_{2,3}$ edges XANES spectra (solid lines), each spectrum area is normalized to 1, linear combinations fits (dashed lines) of normalized spectra of Fe^{2+} reference and Fe^{3+} reference yield the ferric iron percentages.

Fig.8: TEM micrographs and EDX spectra for Illange SPM. A and B: Iron-rich particles, showing hairy texture, mainly constituted of iron oxyhydroxides, calcium phosphates and aluminosilicates (clays). B-1: Typical EDXS spectrum of iron-rich particles (Fe/O close to 0.5) displaying Zn at 2.5%. C: Aluminum oxyhydroxides, calcium phosphates and Zn (6%). D: Zn sulfides, with EDX spectrum (D-1).

Fig.9: STXM experiments for Illange SPM. A and B are high resolution images respectively collected below Fe-$L_{2,3}$ edges (700 eV) and near the maximum of Fe-L_3 edge (710 eV). Dashed lines on B show the regions of interest for spectrum extraction. C: All extracted spectra are identical and after normalization of its area to 1, a linear combinations fit (dashed lines) using normalized spectra of Fe^{2+} reference and Fe^{3+} reference suggests the predominance of a pure Fe^{3+}-oxyhydroxide.

Fig.10: X-ray Micro-Fluorescence on Illange SPM. SPM were prepared as deposit on cellulose filters. Fe and Zn distribution maps acquired at 15 keV, 640 μm per 700 μm, each pixel is 10 μm x 10 μm, counting time is 10 s. The intensities are plotted via a color scale, from the lowest to the highest intensities measured in a selected area, and normalized to a 0-100 scale. Correlation graphs on the left were built from the maps and plot about 4470 dots, except the aberrant and negative values. Correlation factors reported on table 2 were obtained from linear regressions.

Fig.11: Graphical summary. Due to successive steps of selective settling, weathering at the water-sediment interface and remobilization, suspended iron rich particles undergo mineralogical modifications, going from rather ferrous oxides to ferric oxyhydroxides. These modifications provoke a modification of heavy metals (Zn) partitioning between water, suspended solids and sediments. The decrease of Zn in solution is associated with pH values ranging between 7.74 and 7.94, relatively high concentrations in suspended solids (SS in $mg.l^{-1}$) and dissolved organic carbon (DOC in $mg.l^{-1}$). Other physical and chemical parameters were provided on Table 1.

Table 1: Coordinates of sampling stations, physico-chemical parameters, major ions. The measured parameters are compared to mean, maxima and minima values provided by Regional Water Agency (*mean value; MAX; MIN;* SIERM database, 2001-2011 period, http://rhin-meuse.eaufrance.fr/); n.d. : not determined; S.S : suspended solid; DOC : dissolved organic carbon. *For the Illange station (IL), there is no SIERM data.

Table 2: Correlation factors between Fe and Ca, and few metals Zn, Cu and Pb, calculated using linear regression on distribution maps. For Cr, data were not exploitable due to the low level of detection. For the table display, the zones were classified as a function of Zn(Fe) correlation factor, decreasing from Zone 1 to Zone 8. The mean and maximum intensity of Fe K_{α} line (number of counts, with dead time correction) for the zone is also indicated.

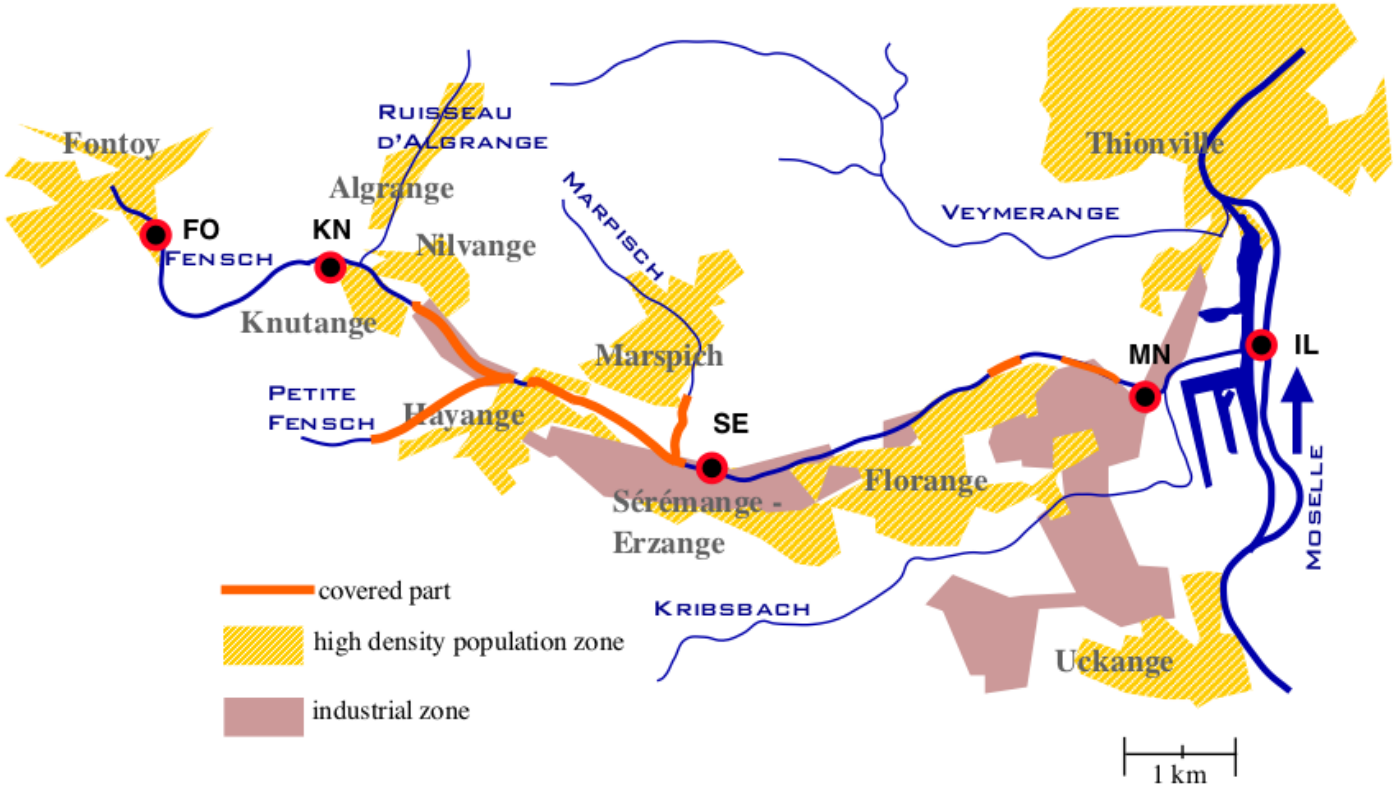
Fontoy
FO
FENSCH
KN
Algrange
RUISSEAU D'ALGRANGE
Nilvange
MARPISCH
Knutange
Marspich
PETITE FENSCH
Hayange
SE
Sérémange - Erzange
Florange
VEYMERANGE
Thionville
MN
IL
MOSELLE
KRIBSBACH
Uckange
covered part
high density population zone
industrial zone
1 km

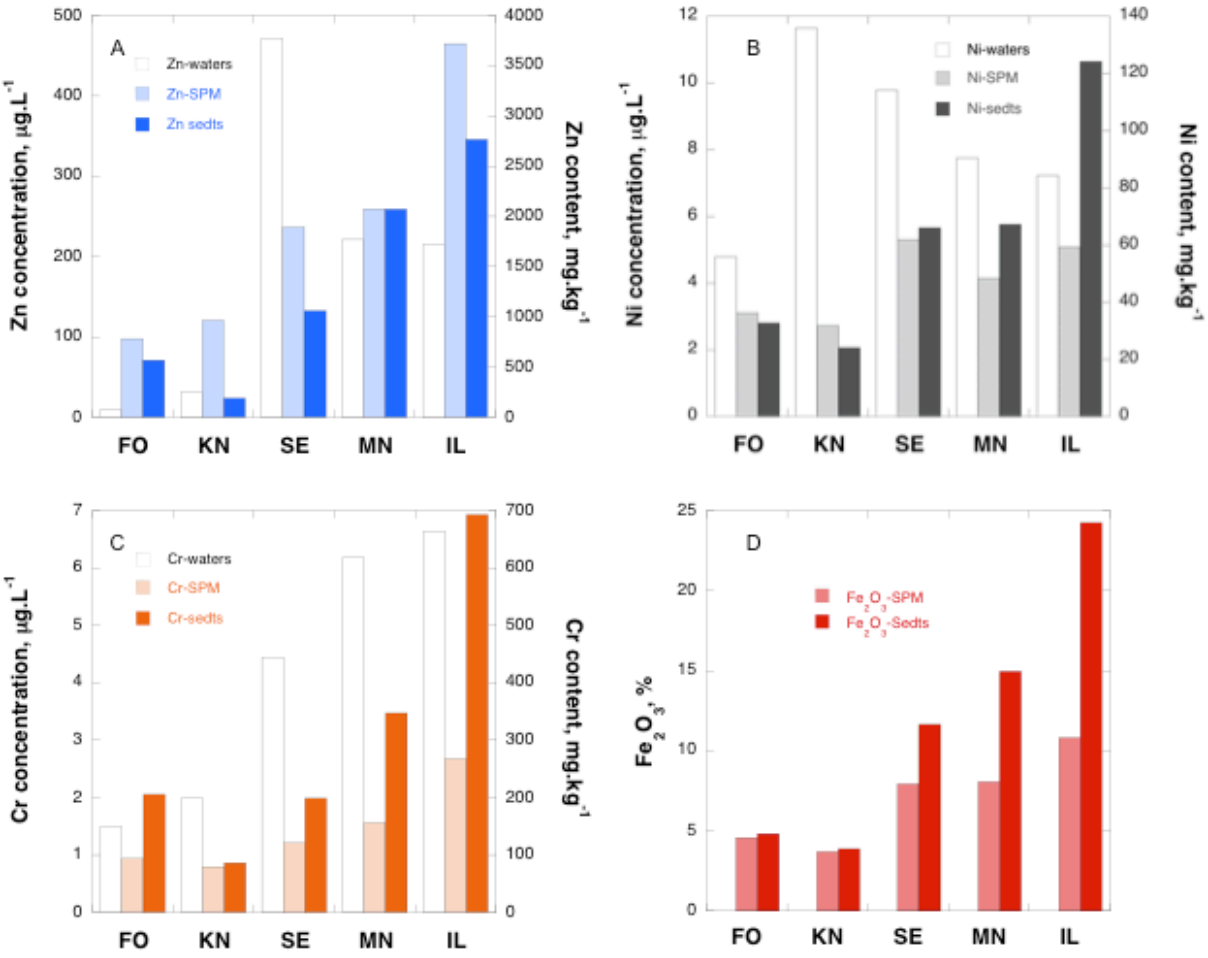
A
Zn-waters
Zn-SPM
Zn sedts
Zn concentration, µg.L-1
Zn content, mg.kg-1
B
Ni-waters
Ni-SPM
Ni-sedts
Ni concentration, µg.L-1
Ni content, mg.kg-1
C
Cr-waters
Cr-SPM
Cr-sedts
Cr concentration, µg.L-1
Cr content, mg.kg-1
D
Fe2O3-SPM
Fe2O3-Sedts
Fe2O3, %
FO
KN
SE
MN
IL

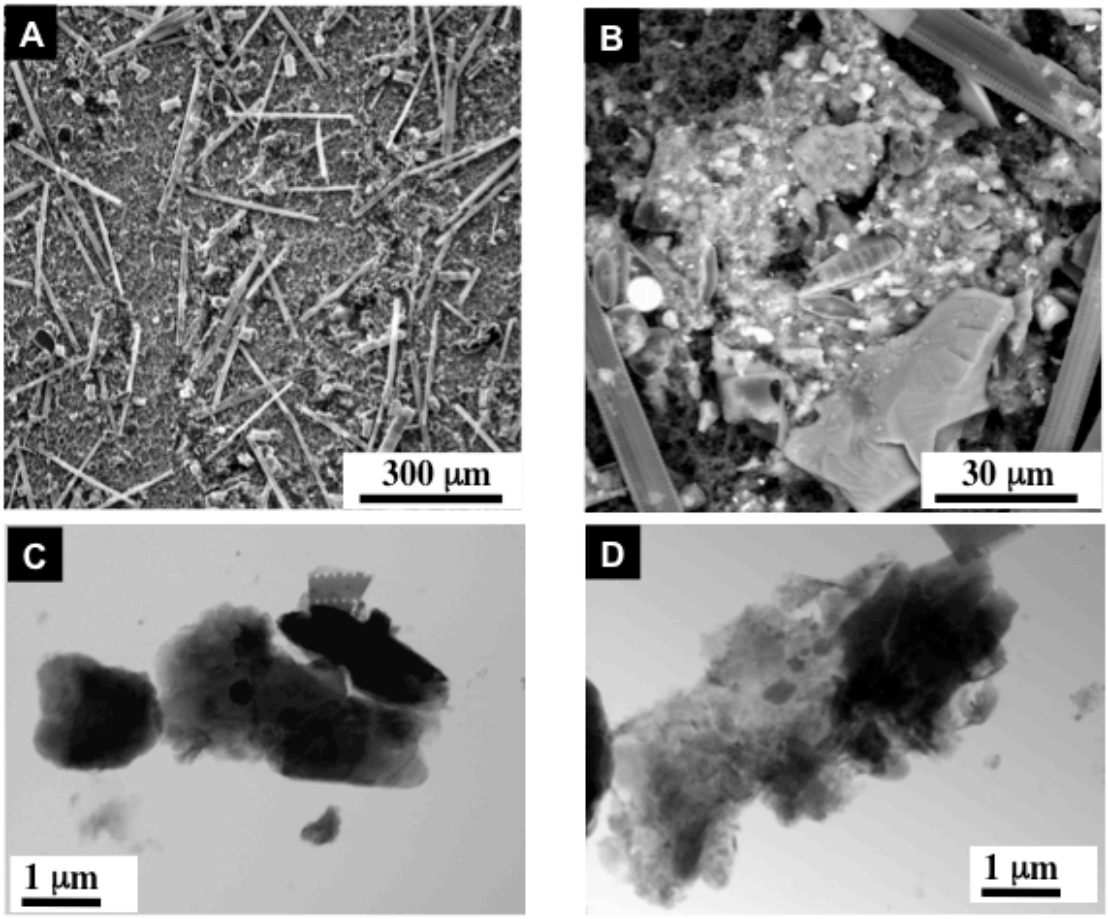
A
300 μm
B
30 μm
C
1 μm
D
1 μm

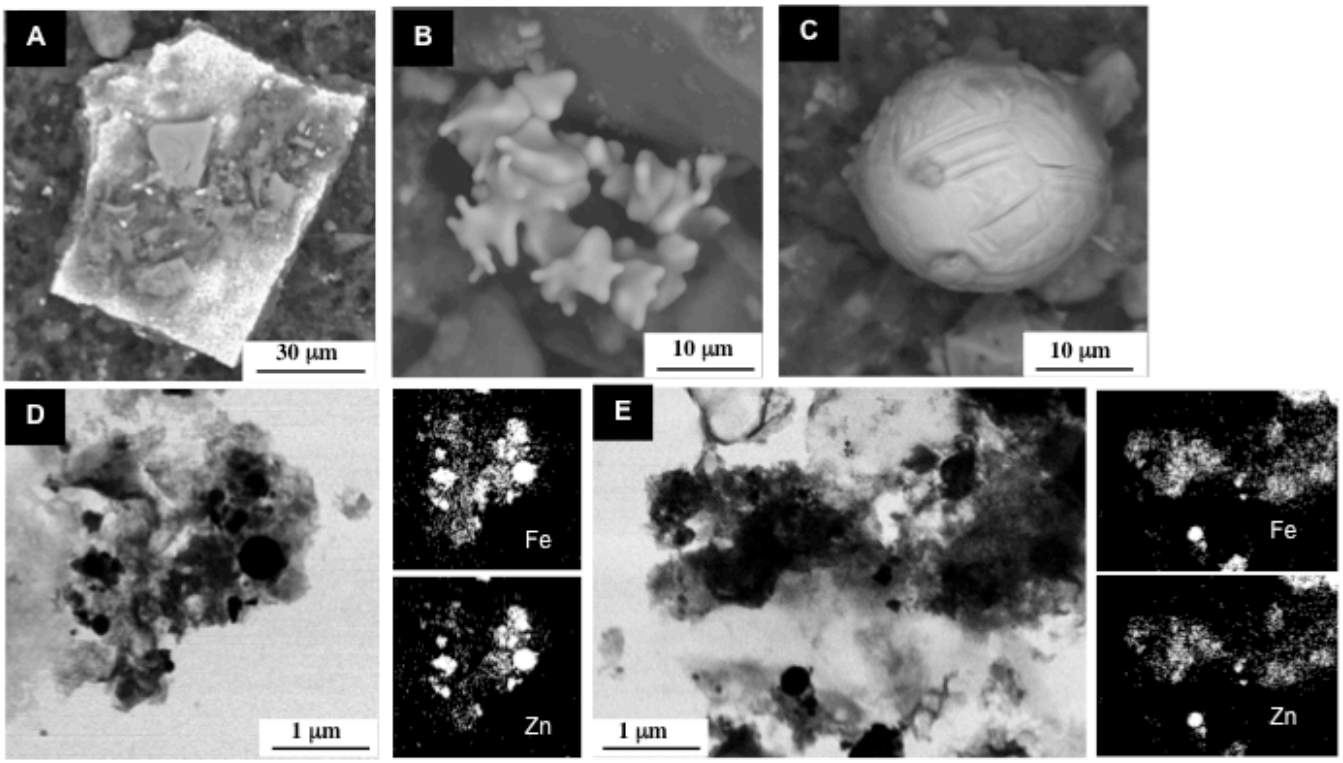
A
30 μm
B
10 μm
C
10 μm
D
1 μm
Fe
Zn
E
1 μm
Fe
Zn

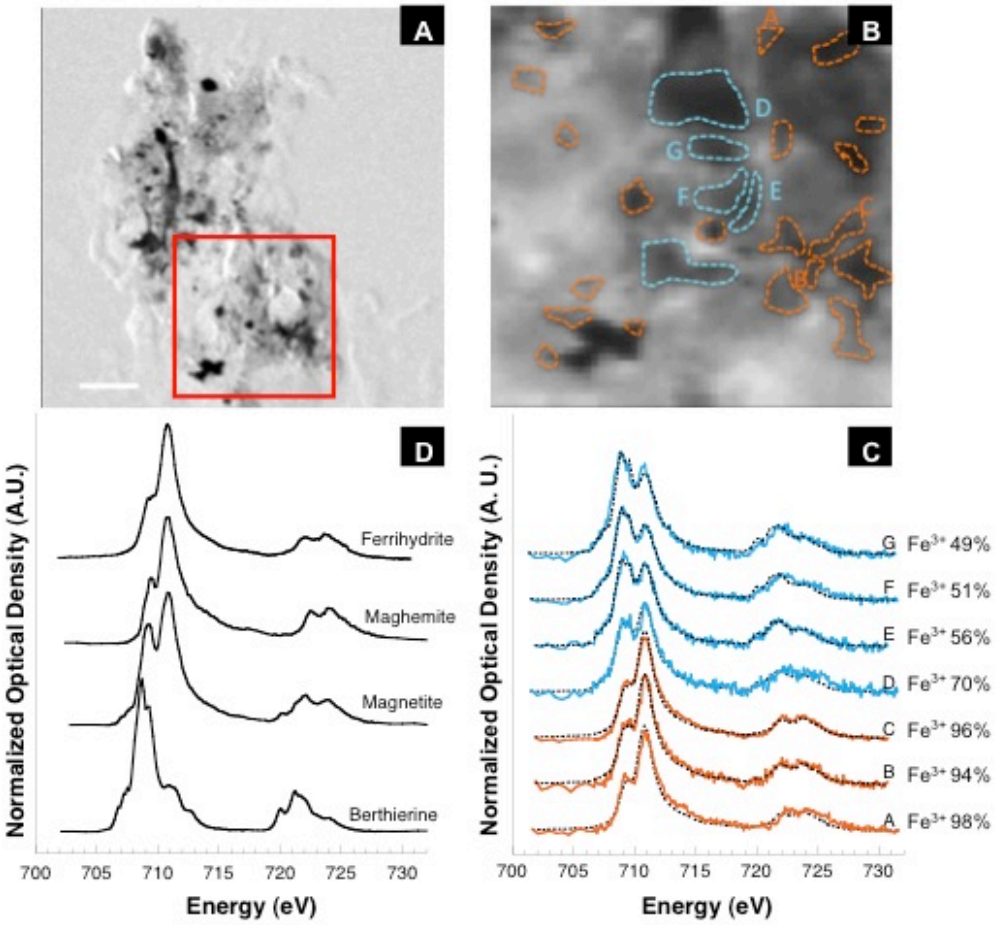
A
B
D
G
F
E
D
Ferrihydrite
Maghemite
Magnetite
Berthierine
Normalized Optical Density (A.U.)
700
705
710
715
720
725
730
Energy (eV)
C
G Fe3+ 49%
F Fe3+ 51%
E Fe3+ 56%
D Fe3+ 70%
C Fe3+ 96%
B Fe3+ 94%
A Fe3+ 98%
Normalized Optical Density (A. U.)
700
705
710
715
720
725
730
Energy (eV)

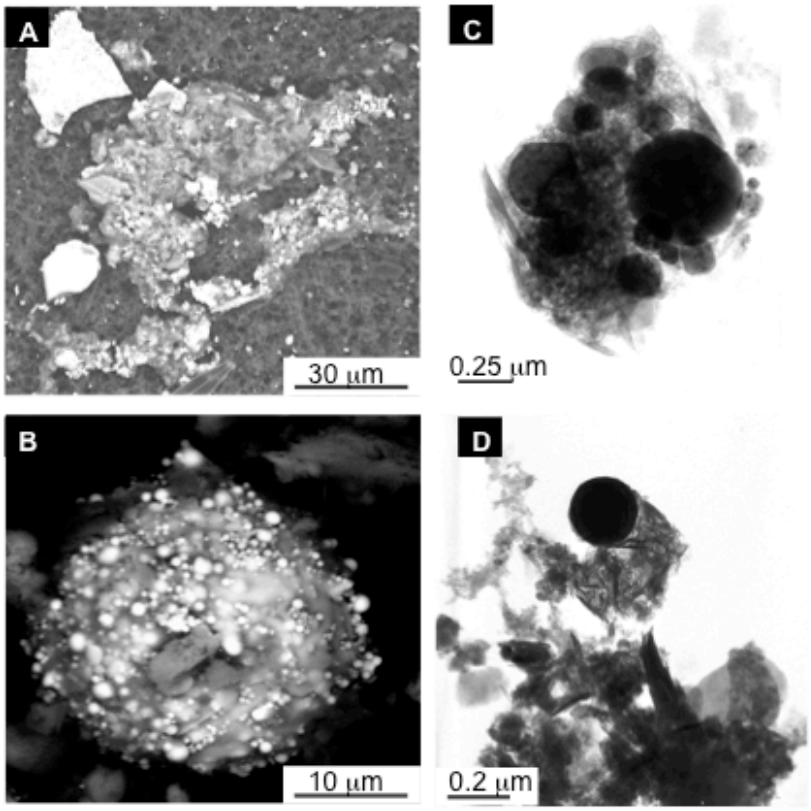
A
30 μm
C
0.25 μm
B
10 μm
D
0.2 μm

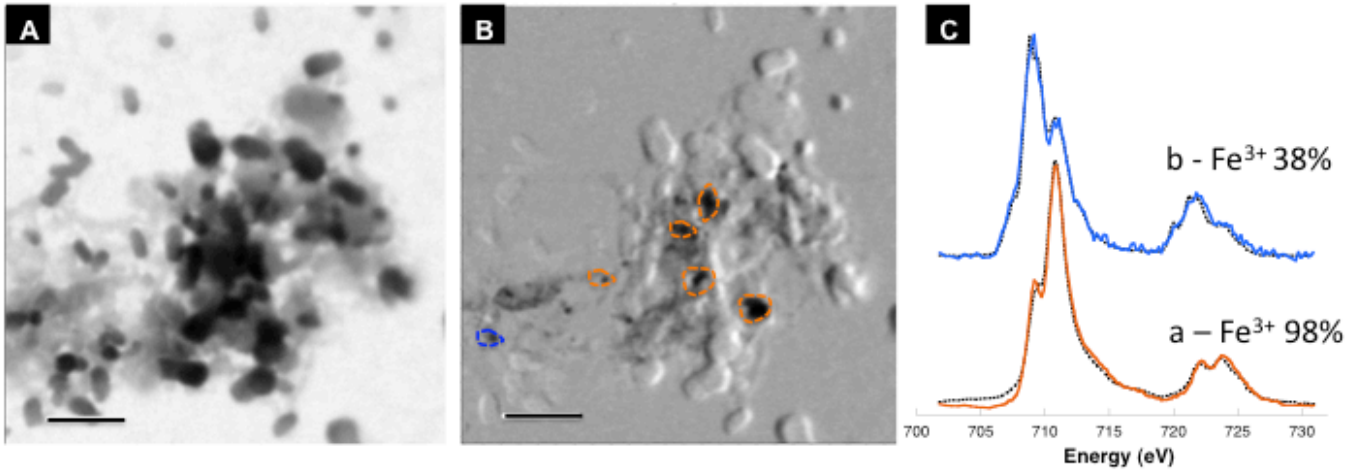
A
B
C
b - Fe3+ 38%
a – Fe3+ 98%
700
705
710
715
720
725
730
Energy (eV)

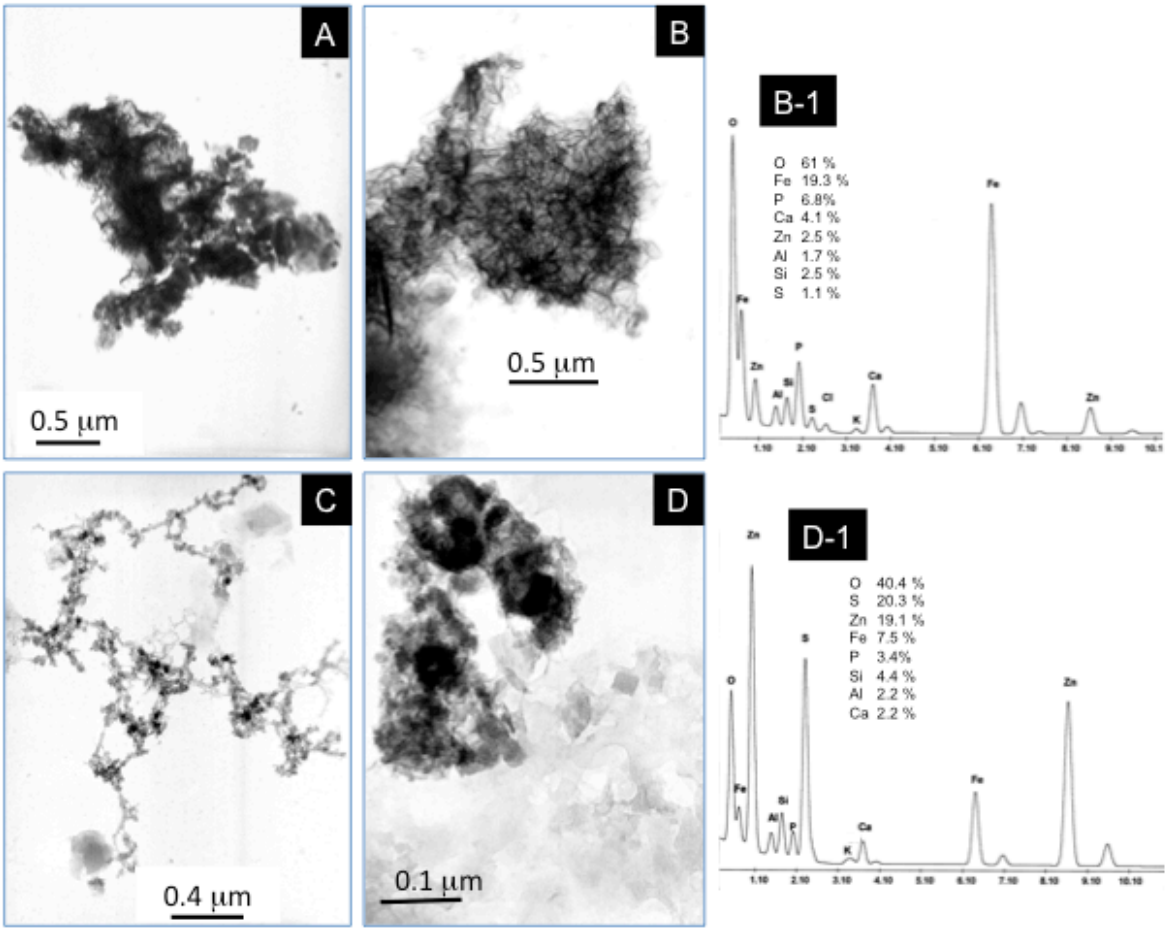
A
0.5 μm
B
0.5 μm
B-1
O 61 %
Fe 19.3 %
P 6.8%
Ca 4.1 %
Zn 2.5 %
Al 1.7 %
Si 2.5 %
S 1.1 %
C
0.4 μm
D
0.1 μm
D-1
O 40.4 %
S 20.3 %
Zn 19.1 %
Fe 7.5 %
P 3.4%
Si 4.4 %
Al 2.2 %
Ca 2.2 %

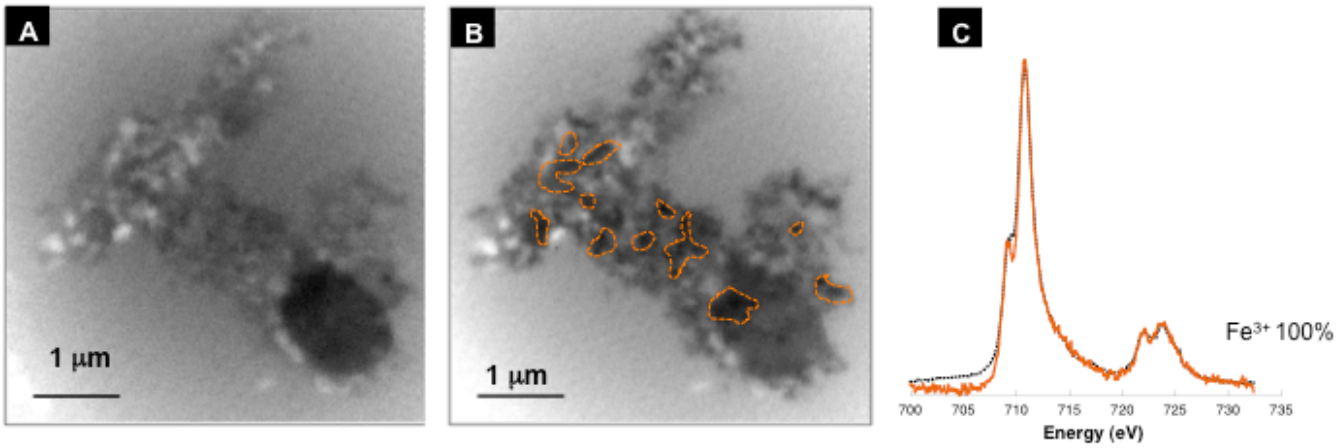
A
1 µm
B
1 µm
C
Fe3+ 100%
700
705
710
715
720
725
730
735
Energy (eV)

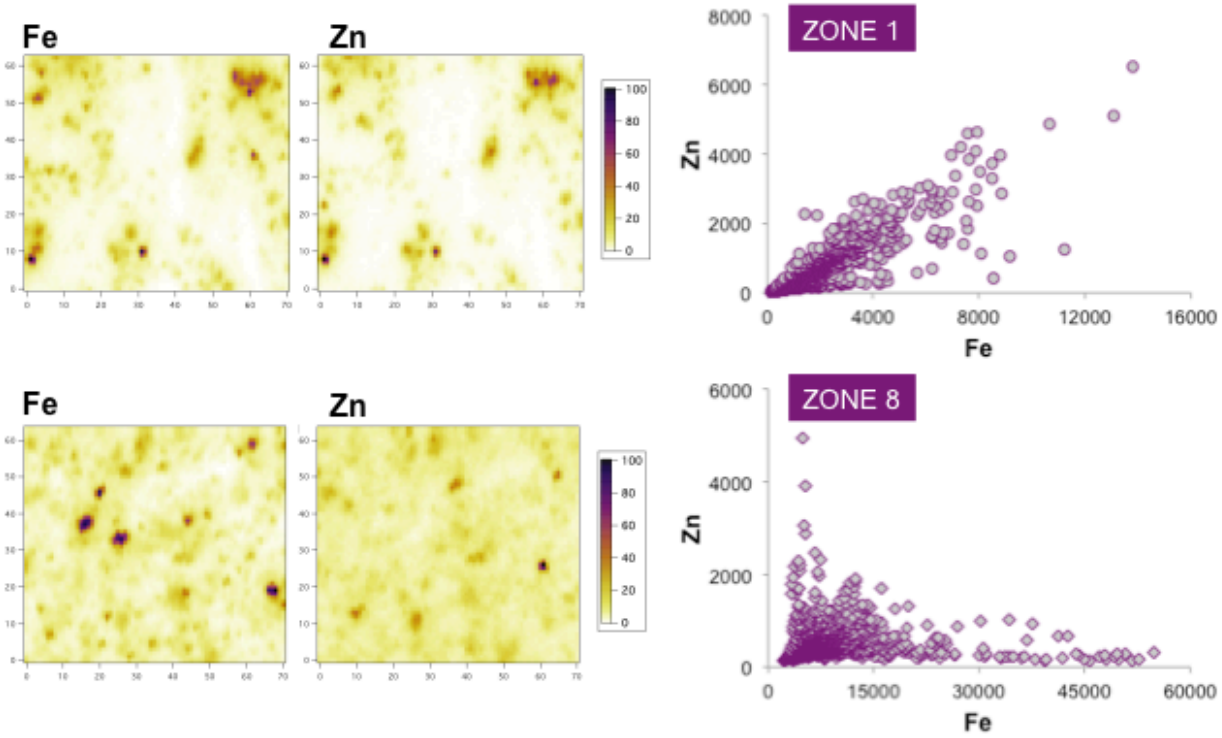
Fe
Zn
100
80
60
40
20
0
ZONE 1
8000
6000
4000
2000
0
Zn
0
4000
8000
12000
16000
Fe
Fe
Zn
100
80
60
40
20
0
ZONE 8
6000
4000
2000
0
Zn
0
15000
30000
45000
60000
Fe

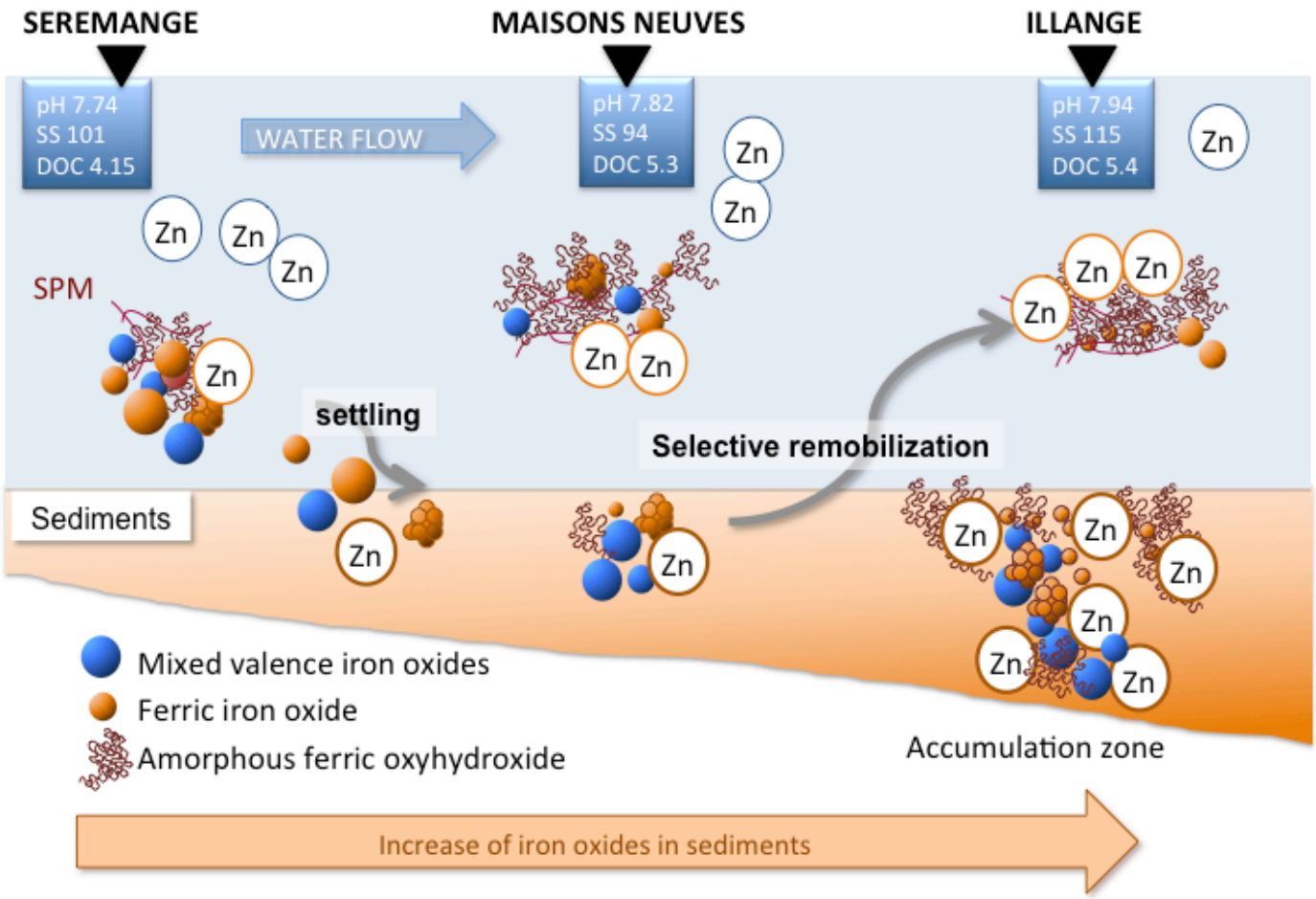
SEREMANGE
MAISONS NEUVES
ILLANGE
pH 7.74
SS 101
DOC 4.15
WATER FLOW
pH 7.82
SS 94
DOC 5.3
pH 7.94
SS 115
DOC 5.4
Zn
SPM
settling
Selective remobilization
Sediments
Mixed valence iron oxides
Ferric iron oxide
Amorphous ferric oxyhydroxide
Accumulation zone
Increase of iron oxides in sediments

Parameter / Station	Fontoy FO	Knutange KN	Seremange SE	Maisons Neuves MN	Illange* IL
Coordinates	49°21'05.0" N 05°59'58.7" E 229 m	49°20'42.2" N 06°01'44.0" E 197 m	49°19'18.6" N 06°05'41.3" E 188 m	49°19'41.4" N 06°09'09.7" E 162 m	49°19'52.4" N 06°09'49.3" E 156 m
Temperature °C	8.7	10.7	5.2	6.5	9.4
Conductivity $\mu S.cm^{-1}$	707	2680	2320	1968	1917
Conductivity SIERM	*633; 725; 422*	*1561; 3193; 560*	*1605; 3205; 623*	*1663; 2658; 416*	-
pH	7.37	7.5	7.74	7.82	7.94
pH SIERM	*8 ± 0.3*	*7.7 ± 0.2*	*8 ± 0.2*	*7.9 ± 0.2*	-
S.S. $mg.L^{-1}$	49	20	101	94	115
S.S. SIERM	*4.4; 50; 1*	*5.6; 170; 1*	*10.3; 93; 2*	*22; 262; 3*	-
DOC $mg.L^{-1}$	2.78	2.66	4.15	5.3	5.42
DOC SIERM	*1.8; 6; 1*	*1.6; 6.5; 0.5*	*2.3; 4.4; 1*	*4; 14; 1*	-
HCO_3 - SIERM	*287.9; 362; 180*	*371.7; 508; 216*	*318; 478; 28*	*288; 453; 176*	-
SO_4 $mg.L^{-1}$	72.4	1138	222	126	92.7
SIERM	*65.4; 160; 21*	*644; 1730;70*	*563.9; 1450; 97*	*427.1; 1070; 96*	-
Cl $mg.L^{-1}$	24.9	45	104	120	125
SIERM	*19.6; 69; 12*	*26.1; 81; 16*	*85.4; 535; 29*	*168.5; 326; 24*	-
NO_3 $mg.L^{-1}$	10.9	2.4	5.0	6.1	7
NO_3 SIERM	*11.8; 50; 1*	*5.2; 15; 0.5*	*6.8; 17; 1*	*7; 16; 1*	-
Ca $mg.L^{-1}$	101.4	287.3	234.0	209.7	211.7
Ca SIERM	*112; 180; 66*	*196.6; 380; 85*	*197; 418; 73*	*179.3; 310; 78*	-
Na $mg.L^{-1}$	26.5	121.6	136.2	107.9	104.2
Na SIERM	*10; 34; 4*	*81; 190; 8*	*90; 213; 23*	*126.5; 220; 30*	-
K $mg.L^{-1}$	2.3	6.2	9.0	9.8	11.9
K SIERM	*2; 6; 1.4*	*4.5; 8; 3*	*15; 77; 4*	*15; 69; 5*	-
Mg $mg.L^{-1}$	10.6	181.1	128.9	91.1	83.8
Al $\mu g.L^{-1}$	5.7	3.9	8.4	6.4	6.7
Si $mg.L^{-1}$	2.4	4.9	4.5	4.8	4.7
Mn $mg.L^{-1}$	0.01	0.4	0.3	0.2	0.2

	Zone 1	Zone 2	Zone 3	Zone 4	Zone 5	Zone 6	Zone 7	Zone 8	Zone 9
Zn/Fe	0.82	0.58	0.42	0.37	0.37	0.29	0.16	0.03	0.02
Pb/Fe	0.65	0.58	0.57	0.44	0.09	0.36	0.36	0.17	0.007
Cu/Fe	0.67	0.59	0.39	0.26	0.04	0.39	0.007	0.06	0.003
Ca/Fe	0.52	0.36	0.19	0.09	0.06	0.36	0.15	0	0
Fe max	13800	15700	62500	60170	53700	34200	57000	55000	64200
Fe moy	970	530	4040	7220	5900	2290	2780	6390	7100

Supplementary Information

1-Evolution of trace and major elements along the Fensch river, supplementary data

The following graphs present the evolution of Cu, Pb, Mn and As concentrations and contents in waters, SPM and sediments along the Fensch linear.

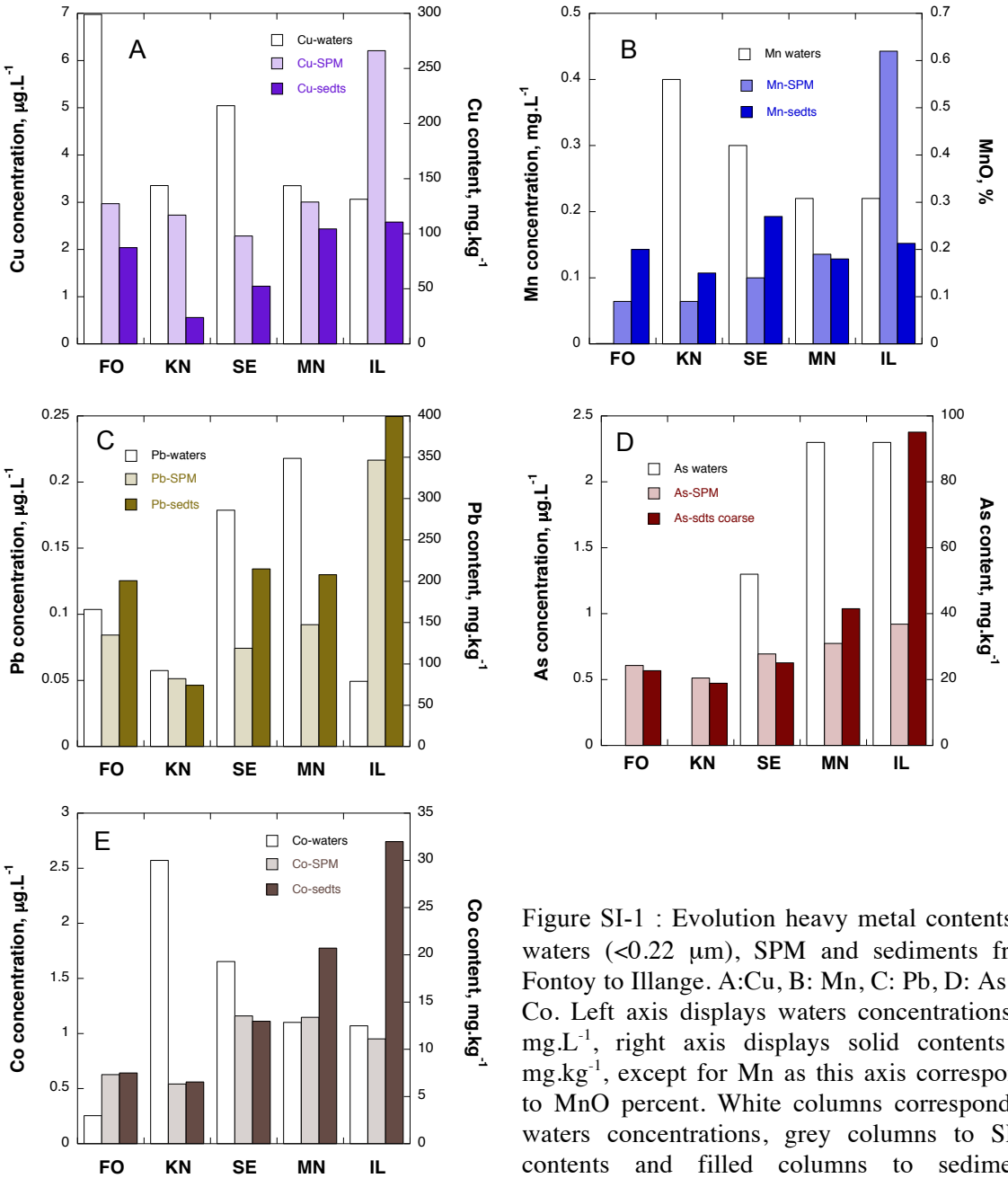

Figure SI-1 : Evolution heavy metal contents in waters (<0.22 µm), SPM and sediments from Fontoy to Illange. A:Cu, B: Mn, C: Pb, D: As, E: Co. Left axis displays waters concentrations in $mg.L^{-1}$, right axis displays solid contents in $mg.kg^{-1}$, except for Mn as this axis corresponds to MnO percent. White columns correspond to waters concentrations, grey columns to SPM contents and filled columns to sediments contents.

Cu, Pb and Mn were considered to belong to Zn group on the basis of the evolution of their contents in SPM. Indeed, for Pb and Cu concentrations in waters do not display strong variations along the river (Pb : 0.05-0.2 $\mu g.L^{-1}$; Cu 3-6 $\mu g.L^{-1}$) but Cu content in SPM (24-266 $mg.kg^{-1}$) present a relatively strong increase in Illange, reaching 266 $mg.kg^{-1}$ for the last station. Pb was also considered as analogous to Zn and Cu, considering that in Illange, Pb content was close in both SPM and sediments (346 $mg.kg^{-1}$ and 400 $mg.kg^{-1}$ respectively).

2-XRD patterns of sediments and SPM

X-ray diffraction data were obtained using a D8 Bruker diffractometer equipped with a (θ, 2θ) goniometer using Co $K_{\alpha 1}$ radiation (λ = 1.7902 Å). X-ray diffractogramms were collected on powder samples in ambient conditions, within the 2Θ range [3, 65°], with 0.036° step and 3s collecting time.

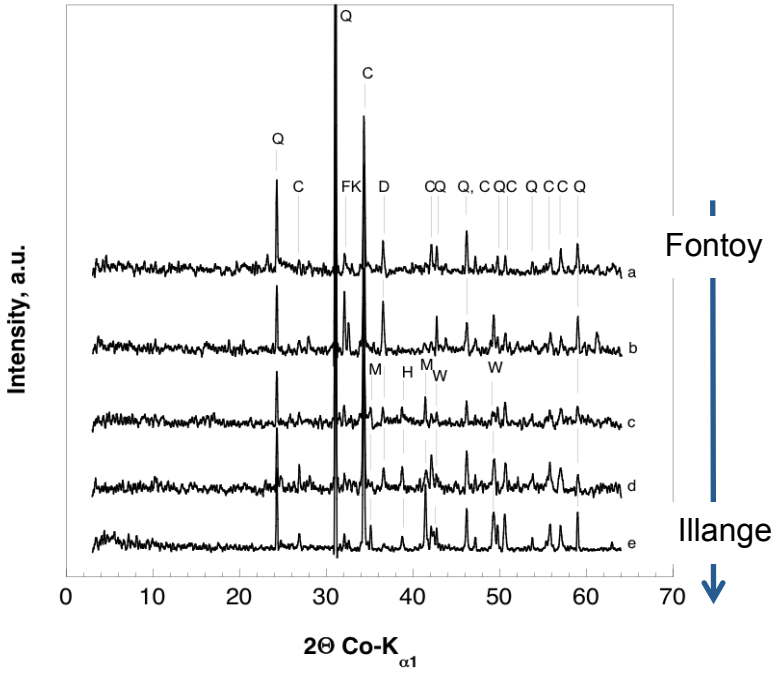

Figure SI-2: Evolution of the X-ray diffractograms obtained on Fensch sediments (0-2mm fraction), a: Fontoy; b: Knutange; c: Seremange; d: Maisons-Neuves; e: Illange. Identified crystalline phases quartz (Q), calcite (C), orthoclase (F_K), dolomite (D), hematite (H), magnetite (M), wuestite (W).

The X-ray diffractograms of the sediments along the Fensch linear confirm the increasing presence of iron-phases. Although XRD analysis does not provide the whole mineralogy of iron phases, it shows that oxides are the predominant crystalline iron phases: magnetite Fe_2O_3, hematite Fe_3O_4 and wuestite FeO.

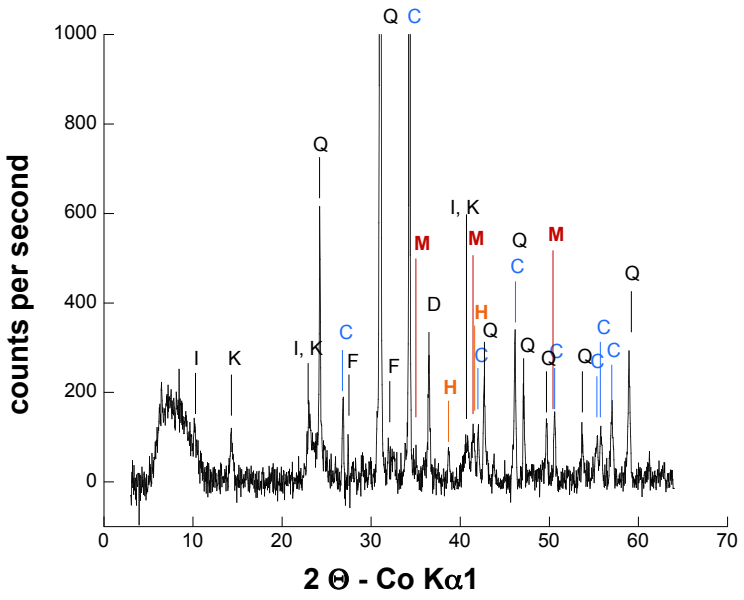

Figure SI-3: X-ray diffractogram obtained on Fensch SPM Seremange;. Identified crystalline phases quartz (Q), calcite (C), orthoclase (F), dolomite (D), hematite (H), magnetite (M), illite (I), kaolinite (K).

The XRD pattern obtained for Seremange SPM presents a very low signal:noise ratio due to the amorphous character of this material. Because the data were collected with few mg of material, the diffraction pattern presents a broad band at low angle values, due to the sample holder. Besides classical minerals such as quartz, calcite that predominates the pattern due to their relatively good cristallinity, hematite and magnetite diffraction bands could be identified (orange and red on the figure SI-3).

3-STEM-EDXS spectra from FONTOY particles

The figure below was obtained on Fensch SPM collected in Fontoy, at the most upstream station on the Fensch linear. For this station, SPM was mainly constituted of diatoms, clay minerals and carbonates. The following figure presents the elemental maps obtained for one particle using STEM-EDXS, as well as one spectrum collected for one point of interest on the particle. The elemental maps, acquired at a nanometer scale, show that the particle is mainly constituted of phyllosilicate layers, illite and smectite clays. The part of diatom skeleton (on the top of the micrograph) provides silicon signal only and a nanometric calcium phosphate could be evidenced and identified through the maps of Ca and P.

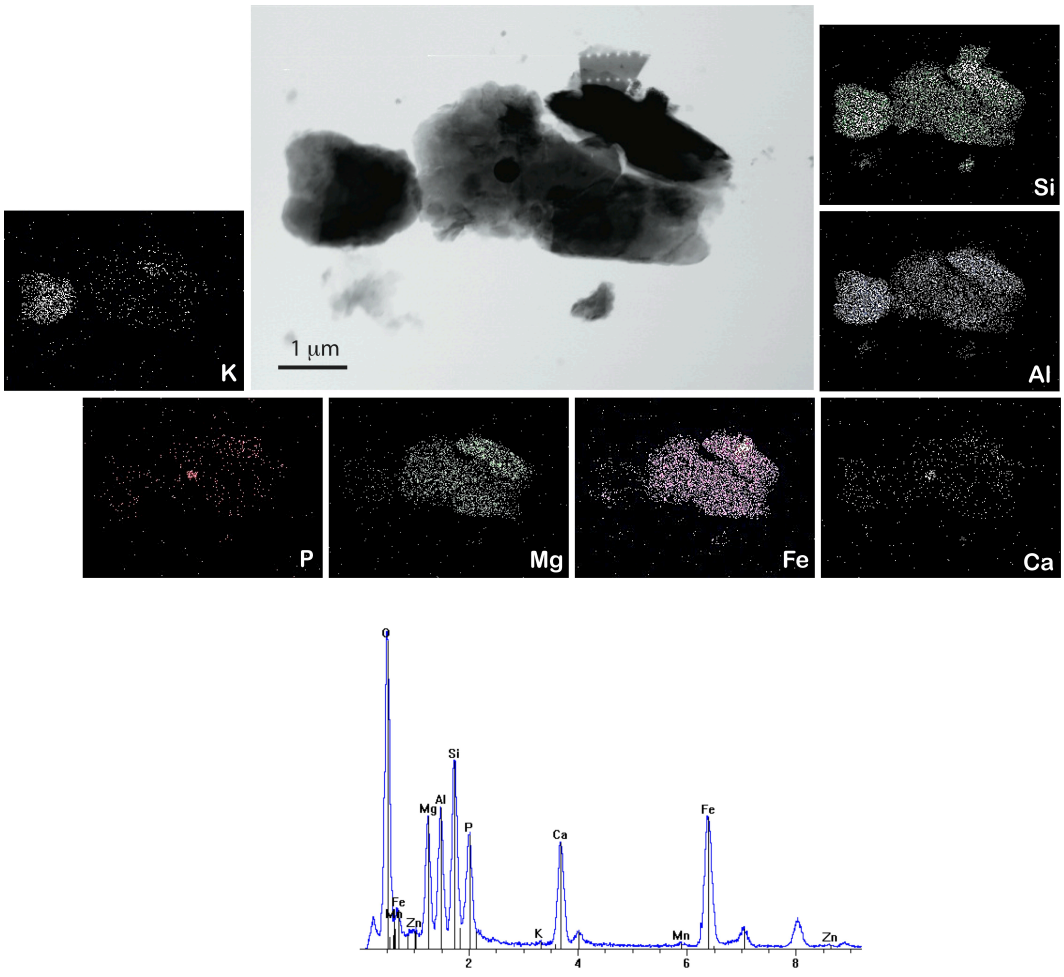

Figure SI-3: Fontoy SPM, STEM micrograph, elemental maps and EDXS spectrum. (scale bar 2.5 µm)